ORIGINAL RESEARCH ARTICLE

Effect of Slag Basicity on Dephosphorization at Lower Basicity and Lower Temperature Based on Industrial Experiments and Ion-Molecular Coexistence Theory

HAN SUN, JIAN YANG, RUN-HAO ZHANG, and WEN-KUI YANG

In the present work, the effect of dephosphorization slag basicity on the dephosphorization of hot metal has been studied in the lower temperature range of 1370 °C to 1420 °C and the lower basicity of 1.26 to 2.20 with new double slag converter steelmaking process (NDSP). Based on the ion-molecule coexistence theory (IMCT), the thermodynamic model IMCT-N_i of dephosphorization slag is established. With increasing basicity from 1.26 to 2.20, the phosphorus distribution ratio L_P between hot metal and slag increases. The dephosphorization ratio and the decarbonization ratio both increase, while the demanganization ratio decreases. The morphologies of P-rich phase change from long strip shape (B = 1.26-1.37) to dendritic shape (B = 1.50) and to massive shape (B = 1.71-2.20). The area of P-rich phase increases from about 4 μm^2 to about 8000 μm^2. The content of P_2O_5 in the P-rich phase increases and the value of the coefficient n in nC_2S-C_3P of the P-rich phase decreases from 6-20 to 1-2. The phosphorus-enrichment contribution ratio of calcium silicate is in the order of $R_{C2S}>R_{CS}>R_{C3S}>R_{C3S2}$. The phosphorus-enrichment degree in dephosphorization slag is enhanced mainly by C_2S-C_3P. With increasing basicity, the calculated results of IMCT-(pct C_2S-C_iP) and R_{C2S} are well consistent with the measurement results of $A^{P\text{-rich phase}}$ and $(\text{pct } P_2O_5)^{P\text{-rich phase}}$ of industrial experiment, indicating that the IMCT calculated results can correctly express the phosphorus-enrichment degree of dephosphorization slag.

https://doi.org/10.1007/s11663-021-02270-y

I. INTRODUCTION

THE multi-refining converter (MURC)[1–3] developed by Nippon Steel in 2001 is a representative new double slag converter steelmaking process(NDSP). Firstly, desiliconization and dephosphorization are carried out at lower basicity and lower temperature in the converter. After intermediate deslagging of dephosphorization slag, the decarburization are conducted in the same converter, with the decarburization slag left in the furnace for dephosphorization in the next heat,[1–5] so that the lime consumption and slag emission amount can be greatly reduced.

Some scholars have studied the effect of dephosphorization slag basicity on hot metal dephosphorization in NDSP. Fang *et al.*[6] optimized the process parameters of the dephosphorization stage in NDSP. When the dephosphorization endpoint temperature is 1328 °C, the dephosphorization slag basicity is 1.5, T.Fe content is 12 to 16 pct, and the oxygen supply intensity is 2.0 to 2.7 m^3/(t min), the dephosphorization ratio reaches 67.3 pct and the phosphorus content reaches 0.011 pct at the endpoint of dephosphorization. Liu *et al.*[7] carried out the industrial experiments on NDSP by 80 t converter. With the slag basicity of 1.2 to 2.0 at the dephosphorization stage, the dephosphorization ratio of hot metal is higher, and the optimal deslagging temperature range is 1327 °C to 1427 °C. Using the hot metal with a high phosphorus content in NDSP, Wang *et al.*[8] showed that with increasing dephosphorization slag basicity from 1.75 to 2.22, the phosphorus content of hot metal decreases linearly at the endpoint of dephosphorization. Based on the 180 ton industrial experiments on NDSP, our previous work[9] studied the behavior of phosphorus enrichment in dephosphorization slag. With increasing basicity, the morphologies of different phases in the

HAN SUN, JIAN YANG, RUN-HAO ZHANG and WEN-KUI YANG are with the State Key Laboratory of Advanced Special Steel, School of Materials Science and Engineering, Shanghai University, Shanghai 200444, P.R. China. Contact e-mail: yang_jian@t.shu.edu.cn
Manuscript submitted 9 April 2021; accepted 23 June 2021.
Article published online July 27, 2021.

dephosphorization slag change greatly, and the area fractions and P_2O_5 content of the P-rich phase also increase.

In the process of dephosphorization in NDSP, the slag is in the coexistence state of solid phase and liquid phase. Many research results[4–17] showed that the phosphorus oxide combines with calcium silicate in slag to form a solid solution, $2CaO{\cdot}SiO_2$-$3CaO{\cdot}P_2O_5$(C_2S-C_3P), which makes phosphorus exist in slag stably. Xie *et al.*[10] studied the crystallization kinetics of C_2S-C_3P solid solution in multiphase slag. The content of C_2S-C_3P solid solution in multiphase slag increases with increasing P_2O_5 content and decreasing holding temperature, and decreases with increasing FeO_t content. They further studied the mass transfer behavior of phosphorus in multiphase dephosphorization slag at 1350 °C by adding P_2O_5 powder into CaO-FeO_t-SiO_2 slag saturated with $2CaO{\cdot}SiO_2$(C_2S).[11] The added P_2O_5 powders can form C_2S-C_3P solid solution rapidly with C_2S in the slag, and the rate control step of the process is the mass transfer of phosphorus from C_2S-C_3P solid solution layer to internal C_2S crystal. Kakimoto *et al.*[12] studied the dissolution behavior of lime in CaO-SiO_2-FeO and CaO-SiO_2-FeO-5.2 pct P_2O_5 slag. Adding P_2O_5 to the slag can promote the dissolution of lime into the slag. The main reason is that part of CaO exists in the slag in the form of C_2S and C_3P in the form of solid solution. Du *et al.*[13] obtained that the distribution ratio of P_2O_5 in solid solution and liquid phase increases with increasing T.Fe content, and has nothing to do with P_2O_5 content and valence of Fe in CaO-SiO_2-FeO-P_2O_5-Na_2O slag.

On the other hand, the ion-molecule coexistence theory (IMCT) is a slag structure theory based on the possible compounds of simple ions, simple molecules and complex molecules in the phase diagram as the structural units, and the mass action law is used to quantitatively calculate the reaction ability of structure units or ion couples in the studied slag.[18–29] The coexistence theory model was first proposed by Chuiko[24] and then was further developed by Zhang.[25]

In recent years, some scholars[22,23,25,26] studied the dephosphorization process of steelmaking slag based on IMCT. Yang *et al.*[22] established the phosphorus distribution ratio prediction model IMCT-logL_P of CaO-FeO-Fe_2O_3-SiO_2-MgO-MnO-Al_2O_3-P_2O_5, and compared the calculation results with the empirical formula values and the measured values. The IMCT-logL_P model can accurately predict the phosphorus distribution ratio of the slag, and the corresponding phosphorus distribution ratio of each component with dephosphorization ability in slag, indicating that C_3P is the main contribution component of L_P, and its contribution ratio is 96.01 pct. They further established the phosphorus capacity prediction model IMCT $-\log C_{PO_4^{3-}}$ and the phosphorus capacity index prediction model IMCT $-\log C_{PO_4^{3-}\ index}$ under the same slag condition based on IMCT.[23] The results show that the dephosphorization reaction is controlled by the basic compositions of converter slag and iron oxide. CaO + Fe_tO is the main contribution component for phosphorus capacity or phosphorus capacity index of slag, and its contribution ratio reaches 99.996 pct. Li *et al.*[26] established the phosphorus distribution ratio model of IMCT-logL_P which can accurately predict the phosphorus distribution ratio of CaO-FeO-Fe_2O_3-SiO_2-MgO steelmaking slag. With increasing CaO and Fe_tO content and decreasing MgO and SiO_2 content, the predicted values of $L_{P,\ cal}$ is increased which is consistent with the measured values.

Based on IMCT, some scholars studied the phosphorus-enrichment capacity of calcium silicate in slag. Xie *et al.*[27] discussed the phosphorus-enrichment capacity of calcium silicate in multiphase slag through the phosphorus-enrichment contribution ratio of calcium silicate R_{Ci} (refer to Eq. [16]) defined by IMCT. In CaO-FeO-Fe_2O_3-SiO_2-MgO-MnO-Al_2O_3-P_2O_5 slag with the temperature of 1350 °C and the basicity of 0.5 to 4, the phosphorus-enrichment contribution ratio of dicalcium silicate R_{C2S} will be significantly increased by increasing the basicity of slag, and the value of R_{C2S} reaches the maximum value when FeO content is 25 pct. In addition, with increasing m(FeO)/m(Fe_2O_3) ratio, the value of R_{C2S} increases, while with increasing P_2O_5 content in slag, the value of R_{C2S} decreases slightly. Li *et al.*[28] studied the phosphorus-enrichment behavior in CaO-FeO-Fe_2O_3-SiO_2-MgO steelmaking slag at 1450 °C to 1600 °C based on IMCT. C_3P formed in slag can combine with C_2S easily to form C_2S-C_3P solid solution at 1500 °C. Under the fixed cooling condition with basicity of 2.5 and the value of (pct Fe_tO)/(pct CaO) of 0.955, the phosphorus-enrichment degree in C_2S-C_3P solid solution $R_{C2S-C3P}$ (refer to Eq. [15]) defined by IMCT is 0.844. They further studied the phosphorus-enrichment behavior in CaO-FeO-Fe_2O_3-SiO_2-MgO slag at 1500 °C and basicity in the range of 1.0 to 2.0.[29] There is an asymmetric inverted V-shape relationship between the enrichment degree of phosphorus in slag and the binary basicity. When the basicity is 1.3, the maximum content of P_2O_5 in C_2S-C_3P solid solution is about 30.0 pct.

From our previous work,[5,9,30,31] the lower temperature range of 1370 °C to 1420 °C and the lower basicity range of 1.26 to 2.20 are the optimal dephosphorization ranges for the NDSP. According to the above literatures, it can be seen that in these temperature and basicity ranges, the researches on the dephosphorization of hot metal and the phosphorus-enrichment capacity of calcium silicate in the dephosphorization slag are quite limited using NDSP.

In the present work, the industrial experiments were carried out by 180 ton top-bottom combined blowing converter for NDSP. When the dephosphorization slag basicity is 1.26 to 2.20 and the dephosphorization endpoint temperature is 1370 °C to 1420 °C, the effect of dephosphorization slag basicity on dephosphorization of hot metal was studied. The effect of dephosphorization slag basicity on the mass action concentration, N_i, of CaO, SiO_2, calcium silicate and phosphate in the dephosphorization slag were analyzed by IMCT-N_i thermodynamic model for CaO-FeO-SiO_2-MgO-MnO-Al_2O_3-P_2O_5 slag. The effect of dephosphorization slag basicity on the enrichment degree R_{Ci-Pj} of P_2O_5

containing solid solution and the phosphorus-enrichment contribution ratio of calcium silicate R_{Ci} were studied. In addition, X-ray diffraction (XRD) was used to detect the phase compositions of dephosphorization slag under different basicities. The morphological evolution of P-rich phase in dephosphorization slag was observed and analyzed by SEM, and the P-rich phase compositions were determined by SEM-EDS under different basicities. Combined with the IMCT thermodynamic calculation results and dephosphorization reaction of molten slag, the effect of dephosphorization slag basicity on phosphorus-enrichment behavior was clarified, which was verified by the experimental analysis results.

II. INDUSTRIAL EXPERIMENTS

A. *New Double Slag Converter Steelmaking Process*

The industrial experiments were carried out with 180 ton top-bottom combined blowing converter in a steelmaking plant of China. Figure 1 shows the NDSP flow chart. The NDSP is mainly divided into eight steps: slag splashing protection → slag solidification confirmation → adding lime and scrap → pouring hot metal → dephosphorization stage → deslagging → decarburization stage → tapping and retaining decarburization slag. According to the silicon content of the hot metal, the quantitatively calculated amounts of auxiliary materials are added in the dephosphorization and decarbonization stages, respectively. Light burned dolomite is used as slag adjusting agent in slag splashing protection.

B. *Industrial Experiment Parameters and Auxiliary Materials*

Table I shows the consumptions of auxiliary materials for 180 ton top-bottom combined blowing converter. Lime is put into the bottom of furnace for preheating before dephosphorization stage, so as to improve the utilization rate of lime. The OG(Oxygen converter Gas recovery) slag pellets contain T.Fe of 55 pct, CaO of 12.4 pct and SiO_2 of 3.8 pct, mainly including the mud produced by oxygen converter gas recovery.

The experimental converter capacity is 180 ton, the actual amount of hot metal added is 186 to 196 t, and the amount of scrap added is 29 to 33 t. Table II shows oxygen flow rates, blowing times, oxygen consumptions in dephosphorization stage and decarburization stage of 180 ton top-bottom combined blowing converter for the heat numbers of S1 to S6. Low-high-low lance position is used for dephosphorization stage blowing. The initial low lance position (1.7 to 1.8 m) promotes oxygen lance ignition, the subsequent high lance position (1.9 to 2.0 m) promotes rapid slagging in the early stage of dephosphorization, and the low lance position (1.65 to 1.75 m) in the later stage of dephosphorization promotes the agitation in dephosphorization. After the dephosphorization stage, the slag is poured out, and then lime, dolomite and other auxiliary materials are added for decarburization blowing. After decarburization, steel is tapped and decarburization slag is left for the dephosphorization of the next heat.

C. *Compositions of the Initial Hot Metal, the Hot Metal at the Endpoint of Dephosphorization and Dephosphorization Slag*

In the smelting process of steel grade Q235B, the hot metal after desulfurization pretreatment is used for dephosphorization. The initial compositions and temperatures of hot metal in 180 ton top-bottom combined blowing converter are shown in Table III.

After the dephosphorization stage, the slag samples were taken from inclined converter by sticking onto a long inserted iron bars, cooling in air and being collected at room temperature. The whole process is very short with about 1 to 2 minutes, so the cooling rate is above 700 °C/ min, especially at the high temperature range. Part of the slag samples were crushed by crusher and

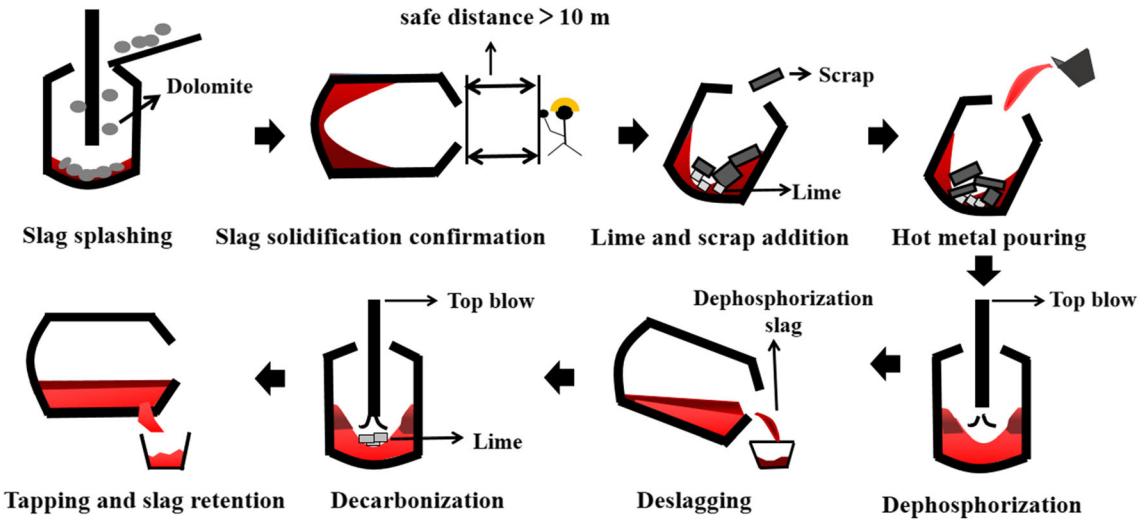

Fig. 1—New double slag converter steelmaking process flow chart.

passed through a 200-mesh sieve to remove the residual iron particles. The compositions of slag samples were analyzed by M4 TORNADO fluorescence spectrometer of Bruker company in Germany. The temperatures were measured and the hot metal was sampled with a sub-gun. Then, the hot metal samples were analyzed by SPECTROMAXx direct reading spectrometer of German SPECTRO company. The basicities and chemical compositions of dephosphorization slag, chemical compositions and temperatures of hot metal at the endpoint of dephosphorization are shown in Table IV. The dephosphorization slag basicity, B, is calculated by binary basicity, which is expressed as Eq. [1]:

$$B = \frac{(\text{pctCaO})}{(\text{pctSiO}_2)} \quad [1]$$

Figure 2 shows the dephosphorization slag compositions with different basicities in $CaO\text{-}SiO_2\text{-}FeO$-8 pct MgO-8 pct MnO-4 pct P_2O_5 pseudo ternary phase diagram. The industrial experiments were carried out at the temperature between 1370 °C and 1420 °C. The liquidus projection sections of dephosphorization slag at 1370 °C and 1420 °C were drawn with FactSage8.0 using the database of phase diagram. The compositions of dephosphorization slags selected in the present work are marked in Figure 2. The compositions of six groups of dephosphorization slag all locate outside the liquidus projection area, which indicates that the dephosphorization slags should be in the multiphase state of solid-liquid coexistence.

The phase analysis of dephosphorization slags were carried out by D8 Advance X-ray powder diffractometer (XRD) of Bruker company in Germany. In the range of $2\theta = 10$ to 90 deg and step size of $0.04°s^{-1}$, XRD data were collected by Cu-Kα radiation. A small amount of massive dephosphorization slag was embedded in epoxy resin. Then it was ground and polished by automatic grinding and polishing machine of PRESI company in France. The surface was carbonized by magnetron sputtering MC1000 of HITACHI company in Japan. The morphology of P-rich phase of dephosphorization slags were observed by Zeiss EVO 18 electronic scanning microscope of Zeiss company of Germany, and the chemical compositions of P-rich phase in dephosphorization slags were analyzed by X-Max^N large area energy dispersive spectrometer (SEM-EDS) of Oxford Instruments Company in UK.

III. THERMODYNAMIC MODEL IMCT-N_I FOR CALCULATING MASS ACTION CONCENTRATIONS OF STRUCTURAL UNITS OR ION COUPLES IN $CAO\text{-}SIO_2\text{-}FEO\text{-}MGO\text{-}MNO\text{-}P_2O_5\text{-}AL_2O_3$ SLAGS

A. *Hypotheses*

According to the classical hypothesis of IMCT summarized by Zhang *et al.*[25] and Yang *et al.*,[22] in the thermodynamic model IMCT-N_i for calculating the mass action concentration of structural unit or ion couple in the dephosphorization slag of $CaO\text{-}SiO_2\text{-}FeO\text{-}MgO\text{-}MnO\text{-}P_2O_5\text{-}Al_2O_3$ which reacts with hot metal, the main assumptions can be summarized as follows:

In the dephosphorization slag in the NDSP, the structural units Ca^{2+}, Mg^{2+}, Fe^{2+}, Mn^{2+} and O^{2-} exist as simple ions, SiO_2, P_2O_5 and Al_2O_3 exist as simple molecules; silicate and phosphate are complex molecules. Each structural unit has its own position in the dephosphorization slag.
Each kind of cation and anion generated by the same component will participate in the chemical reaction of forming complex molecules in the form of ($Me^{2+} + O^{2-}$) ion couple. The chemical reaction of forming complex molecule obeys the mass action law.
The structural units in dephosphorization slag which reacts with hot metal have continuity in the studied concentration range.
The reaction between simple ions and simple molecules to form complex molecules by bonding ion couples is in chemical dynamic equilibrium.

B. *Selection of Structural Units in $CaO\text{-}SiO_2\text{-}FeO\text{-}MgO\text{-}MnO\text{-}P_2O_5\text{-}Al_2O_3$ Dephosphorization Slag*

At the endpoint of the dephosphorization stage in the NDSP, the dephosphorization slag containing phosphorus reacted with hot metal is chosen as $CaO\text{-}FeO\text{-}SiO_2\text{-}MgO\text{-}MnO\text{-}Al_2O_3\text{-}P_2O_5$. According to the binary and ternary phase diagrams[25] of $CaO\text{-}SiO_2$, $MgO\text{-}SiO_2$, $FeO\text{-}SiO_2$, $MnO\text{-}SiO_2$, $MgO\text{-}P_2O_5$, $CaO\text{-}P_2O_5$, $FeO\text{-}P_2O_5$, $MnO\text{-}P_2O_5$, $CaO\text{-}Al_2O_3$, $CaO\text{-}MgO\text{-}SiO_2$, $CaO\text{-}Al_2O_3\text{-}MgO$, etc., and other binary and ternary phase diagrams related to dephosphorization slag, it is found that there are 32 complex molecules in dephosphorization slag, such as $CaO{\cdot}SiO_2$, $3CaO{\cdot}P_2O_5$, $2FeO{\cdot}SiO_2$. In Table V, all simple ions, simple molecules and complex molecules in $CaO\text{-}FeO\text{-}SiO_2\text{-}MgO\text{-}MnO\text{-}Al_2O_3\text{-}P_2O_5$ dephosphorization slag at 1370 °C to 1420 °C are summarized and assigned specific numbers.

In 100 g dephosphorization slag of $CaO\text{-}FeO\text{-}SiO_2\text{-}MgO\text{-}MnO\text{-}Al_2O_3\text{-}P_2O_5$, the initial mole numbers of seven components are expressed as $a_1 = n^0_{CaO}$, $a_2 = n^0_{MnO}$, $a_3 = n^0_{MgO}$, $a_4 = n^0_{FeO}$, $b_1 = n^0_{SiO_2}$, $b_2 = n^0_{P_2O_5}$, $b_3 = n^0_{Al_2O_3}$, respectively. The total equilibrium mole number $\sum n_i$ of all structural units can be expressed as Eq. [2].

$$\sum n_i = 2n1 + 2n2 + 2n3 + 2n4 + n5 + n6 + n7 + nc1 + nc2 + \cdots + nc32 \quad [2]$$

According to the definition of mass action concentration N_i[18–29] of structural unit or ion couples in slag, N_i is the ratio of equilibrium mole number of structural unit i to the total equilibrium mole numbers $\sum N_i$ of all structural units in slag with a fixed amount. The calculation formula of mass action concentration of structural unit i and ion couples ($Me^{2+} + O^{2-}$) in slag is expressed as Eqs. [3] and [4].[22,23,25]

Table I. Consumptions of Auxiliary Materials of 180 Ton Top-Bottom Combined Blowing Converter

Auxiliary Materials	During Slag Splashing	De-P Process	De-C Process
Lime (t)	2.44-3.12	0	3.06-4.86
Dolomite (t)	0.86-1.11	0	0.23-1.37
Magnesite (t)	0	0	1.62-2.53
OG ball (t)	0	2.02-2.53	0
Sinter (t)	0	0.56-1.01	0.62-3.21
Slag steel (t)	0	11.74-12.66	0

Table II. Oxygen Flow Rates, Blowing Times, Oxygen Consumptions in Dephosphorization Stage and Decarburization Stage

	De-P Stage			De-C Stage		
Heats	O_2 Flow Rate (Nm^3/h)	Time (s)	O_2 Consumption (Nm^3)	O_2 Flow Rate (Nm^3/h)	Time (s)	O_2 Consumption (Nm^3)
S1	35800	330	3282	38017	641	6769
S2	37092	317	3266	37576	675	7045
S3	37535	324	3378	39817	658	7277
S4	36661	331	3370	37661	661	6914
S5	36122	327	3281	37985	680	7174
S6	34827	345	3337	40394	633	7102

Table III. Initial Compositions and Temperatures of Hot Metal in 180 Ton Top-Bottom Combined Blowing Converter

Sample	[Pct C]	[Pct Si]	[Pct Mn]	[Pct S]	[Pct P]	T (°C)
S1	4.647	0.360	0.270	0.004	0.156	1345
S2	4.647	0.430	0.240	0.020	0.161	1361
S3	4.653	0.380	0.280	0.030	0.146	1350
S4	4.651	0.310	0.250	0.006	0.142	1351
S5	4.650	0.210	0.240	0.008	0.168	1340
S6	4.651	0.450	0.230	0.009	0.142	1359

Table IV. Basicities and Chemical Compositions of Dephosphorization Slags, Chemical Compositions and Temperatures of Hot Metal at the Endpoint of Dephosphorization

	Basicities and Chemical Compositions of Dephosphorization Slags (Pct)								Chemical Compositions of Hot Metal (Pct)					
Sample	B	CaO	SiO_2	MgO	MnO	FeO	P_2O_5	Al_2O_3	[C]	[Si]	[Mn]	[P]	[S]	T (°C)
S1	1.26	33.242	26.306	7.097	10.944	18.343	2.149	1.919	3.324	0.012	0.087	0.134	0.016	1375
S2	1.37	33.977	24.787	9.507	8.571	18.925	2.853	1.380	3.274	0.012	0.078	0.103	0.023	1420
S3	1.50	36.460	24.389	6.433	9.671	17.954	3.175	1.918	3.240	0.010	0.093	0.065	0.011	1370
S4	1.71	36.480	21.278	7.617	8.963	19.972	3.682	2.008	3.179	0.009	0.102	0.057	0.022	1400
S5	1.90	37.628	19.814	7.596	9.607	17.043	5.099	3.213	3.112	0.001	0.124	0.065	0.028	1373
S6	2.20	40.257	18.308	9.301	5.734	20.476	3.904	2.020	3.072	0.026	0.148	0.048	0.020	1419

$$N_i = \frac{n_i}{\sum n_i} \quad [3]$$

$$N_{MeO} = N_{Me^{2+},MeO} + N_{O^{2-},MeO} = \frac{n_{Me^{2+},MeO} + n_{O^{2-},MeO}}{\sum n_i} = \frac{2n_{MeO}}{\sum n_i} \quad [4]$$

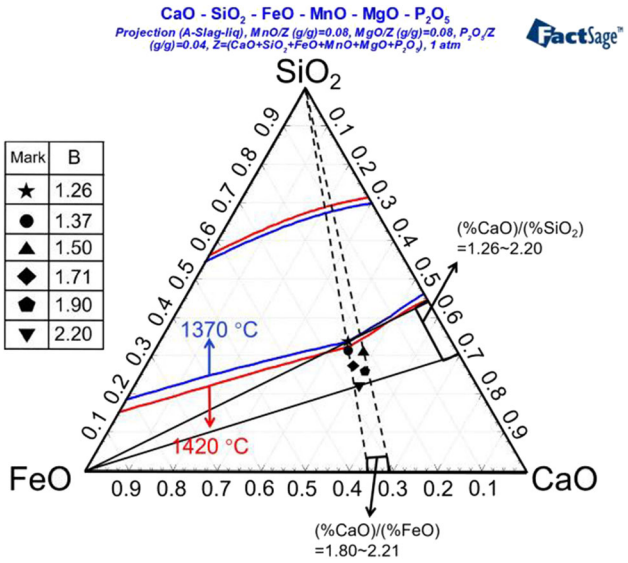

Fig. 2—Dephosphorization slag compositions with different basicities in CaO-SiO_2-FeO-8 pct MgO-8 pct MnO-4 pct P_2O_5 pseudo ternary phase diagram.

Table V also lists the ion couples formed by simple ions in the dephosphorization slag of CaO-FeO-SiO_2-MgO-MnO-Al_2O_3-P_2O_5, as well as the equilibrium mole number n_i of simple ions, simple and complex molecules and the corresponding mass action concentration N_i.

The chemical reaction for the formation of 32 complex molecules ci in the dephosphorization slag of CaO-FeO-SiO_2-MgO-MnO-Al_2O_3-P_2O_5 are listed in Table VI, and the relationship between the variation of standard molar Gibbs free energy $\Delta_r G^{\Theta}_{m,ci}$ and temperature T are also given. The expressions of the corresponding standard reaction equilibrium constants K^{Θ}_{ci} are also listed in Table VI. In addition, the mass action concentrations N_{ci} for all complex molecules expressed using N_1 (N_{CaO}), N_2 (N_{MnO}), N_3 (N_{MgO}), N_4 (N_{FeO}), N_5 (N_{SiO_2}), N_6 ($N_{P_2O_5}$), N_7 (N_{Al2O3}) and K^{Θ}_{ci} are summarized in Table VI.

C. *Establishment of IMCT-N_i Thermodynamic Model for Calculating Mass Action Concentrations of Structural Units or Ion Couples in CaO-FeO-SiO_2-MgO-MnO-Al_2O_3-P_2O_5 Dephosphorization Slag*

With the dephosphorization reaction going on, the phosphorus in hot metal gradually enters the dephosphorization slag and partially removed at the end of dephosphorization stage. Combined with IMCT, N_i and $\sum n_i$ in Tables V and VI, the mass conservation equations of seven components in 100 g dephosphorization slag of CaO-FeO-SiO_2-MgO-MnO-Al_2O_3-P_2O_5 are established, which are expressed as Eqs. [5] through [11], respectively.

$$\begin{aligned}a_1 = (0.5N_1 + N_{c1} + 2N_{c2} + 3N_{c3} + 3N_{c4} + 3N_{c5} + N_{c6} + N_{c7} + N_{c8} \\ +12N_{c9} + 2N_{c19} + N_{c20} + N_{c21} + N_{c22} + 2N_{c23} + 3N_{c24} + 2N_{c26} + 3N_{c27} \\ +4N_{c28})\sum n_i = (0.5N_1 + K^{\Theta}_{c1}N_1N_5 + 2K^{\Theta}_{c2}N_1^2N_5 + 3K^{\Theta}_{c3}N_1^3N_5 + 3K^{\Theta}_{c4}N_1^3N_5^2 \\ +3K^{\Theta}_{c5}N_1^3N_7 + K^{\Theta}_{c6}N_1N_7 + K^{\Theta}_{c7}N_1N_7^2 + K^{\Theta}_{c8}N_1N_7^6 + 12K^{\Theta}_{c9}N_1^{12}N_7^7 + 2K^{\Theta}_{c19}N_1^2N_5N_7 \\ +K^{\Theta}_{c20}N_1N_5^2N_7 + K^{\Theta}_{c21}N_1N_3N_5 + K^{\Theta}_{c22}N_1N_3N_5^2 + 2K^{\Theta}_{c23}N_1^2N_3N_5^2 + 3K^{\Theta}_{c24}N_1^3N_3N_5^2 \\ +2K^{\Theta}_{c26}N_1^2N_6 + 3K^{\Theta}_{c27}N_1^3N_6 + 4K^{\Theta}_{c28}N_1^4N_6)\sum n_i = n^0_{CaO}(\text{mol})\end{aligned} \quad [5]$$

$$\begin{aligned}a_2 = (0.5N_2 + 2N_{c15} + N_{c16} + N_{c17})\sum n_i \\ = (0.5N_2 + 2K^{\Theta}_{c15}N_2^2N_5 + K^{\Theta}_{c16}N_2N_5 + K^{\Theta}_{c17}N_2N_7)\sum n_i = n^0_{MnO}(\text{mol})\end{aligned} \quad [6]$$

$$\begin{aligned}a_3 = (0.5N_3 + N_{c10} + 2N_{c11} + N_{c12} + N_{c21} + N_{c22} + N_{c23} + N_{c24} \\ +2N_{c25} + 2N_{c31} + 3N_{c32})\sum n_i = (0.5N_3 + K^{\Theta}_{c10}N_3N_5 + 2K^{\Theta}_{c11}N_3^2N_5 \\ +K^{\Theta}_{c12}N_3N_7 + K^{\Theta}_{c21}N_1N_3N_5 + K^{\Theta}_{c22}N_1N_3N_5^2 + K^{\Theta}_{c23}N_1^2N_3N_5^2 + K^{\Theta}_{c24}N_1^3N_3N_5^2 \\ +2K^{\Theta}_{c25}N_3^2N_5^5N_7^2 + 2K^{\Theta}_{c31}N_3^2N_6 + 3K^{\Theta}_{c32}N_3^3N_6)\sum n_i = n^0_{MgO}(\text{mol})\end{aligned} \quad [7]$$

$$\begin{aligned}a_4 = (0.5N_4 + 2N_{c13} + N_{c14} + 3N_{c29} + 4N_{c30})\sum n_i \\ = (0.5N_4 + 2K^{\Theta}_{c13}N_4^2N_5 + K^{\Theta}_{c14}N_4N_7 + 3K^{\Theta}_{c29}N_4^3N_6 + 4K^{\Theta}_{c30}N_4^4N_6)\sum n_i = n^0_{FeO}(\text{mol})\end{aligned} \quad [8]$$

$$\begin{aligned}b_1 = (N_5 + N_{c1} + N_{c2} + N_{c3} + 2N_{c4} + N_{c10} + N_{c11} + N_{c13} + N_{c15} \\ +N_{c16} + 2N_{c18} + N_{c19} + 2N_{c20} + N_{c21} + 2N_{c22} + 2N_{c23} + 2N_{c24} + 5N_{c25})\sum n_i \\ = (N_5 + K^{\Theta}_{c1}N_1N_5 + K^{\Theta}_{c2}N_1^2N_5 + K^{\Theta}_{c3}N_1^3N_5 + 2K^{\Theta}_{c4}N_1^3N_5^2 + K^{\Theta}_{c10}N_3N_5 \\ +K^{\Theta}_{c11}N_3^2N_5 + K^{\Theta}_{c13}N_4^2N_5 + K^{\Theta}_{c15}N_2^2N_5 + K^{\Theta}_{c16}N_2N_5 + 2K^{\Theta}_{c18}N_2^2N_7^2 \\ +K^{\Theta}_{c19}N_1^2N_5N_7 + 2K^{\Theta}_{c20}N_1N_5^2N_7 + K^{\Theta}_{c21}N_1N_3N_5 + 2K^{\Theta}_{c22}N_1N_3N_5^2 \\ +2K^{\Theta}_{c23}N_1^2N_3N_5^2 + 2K^{\Theta}_{c24}N_1^3N_3N_5^2 + 5K^{\Theta}_{c25}N_3^2N_5^5N_7^2)\sum n_i = n^0_{SiO_2}(\text{mol})\end{aligned} \quad [9]$$

$$\begin{aligned}b_2 = (N_6 + N_{c26} + N_{c27} + N_{c28} + N_{c29} + N_{c30} + N_{c31} + N_{c32})\sum n_i \\ = (N_6 + K^{\Theta}_{c26}N_1^2N_6 + K^{\Theta}_{c27}N_1^3N_6 + K^{\Theta}_{c28}N_1^4N_6 + K^{\Theta}_{c29}N_4^3N_6 \\ +K^{\Theta}_{c30}N_4^4N_6 + K^{\Theta}_{c31}N_3^2N_6 + K^{\Theta}_{c32}N_3^3N_6)\sum n_i = n^0_{P_2O_5}(\text{mol})\end{aligned} \quad [10]$$

$$\begin{aligned}b_3 = (N_7 + N_{c5} + N_{c6} + 2N_{c7} + 6N_{c8} + 7N_{c9} + N_{c12} + N_{c14} + N_{c17} \\ +3N_{c18} + N_{c19} + 2N_{c20} + 2N_{c25})\sum n_i \\ = (N_7 + K^{\Theta}_{c5}N_1^3N_7 + K^{\Theta}_{c6}N_1N_7 + 2K^{\Theta}_{c7}N_1N_7^2 + 6K^{\Theta}_{c8}N_1N_7^6 \\ +7K^{\Theta}_{c9}N_1^{12}N_7^7 + K^{\Theta}_{c12}N_3N_7 + K^{\Theta}_{c14}N_4N_7 + K^{\Theta}_{c17}N_2N_7 + 3K^{\Theta}_{c18}N_5^2N_7^3 \\ +K^{\Theta}_{c19}N_1^2N_5N_7 + K^{\Theta}_{c20}N_1N_5^2N_7 + 2K^{\Theta}_{c25}N_3^2N_5^5N_7^2)\sum n_i = n^0_{Al_2O_3}(\text{mol})\end{aligned} \quad [11]$$

According to the mass conservation law, the sum of mole fractions of all structural units in the dephosphorization slag of CaO-FeO-SiO_2-MgO-MnO-Al_2O_3-P_2O_5 with fixed total mass under equilibrium condition is equal to 1.0, and Eq. [12] can be obtained.

Table V. Expression of Structural Units as Ion Couples, Simple or Complex Molecules, Their Numbers, Mole Numbers and Mass Action Concentration of N_i in 100 g Dephosphorization Slag of CaO-FeO-SiO_2-MgO-MnO-Al_2O_3-P_2O_5 Based on the IMCT

Item	Structural Units as Ion Couples or Molecules	Number	Mole Number of Structural Units or Ion Couples	Mass Action Concentration of Structural Units or Ion Couple
Simple cation and anion (4)	$Ca^{2+} + O^{2-}$	1	$n_1 = n_{Ca^{2+},CaO} = n_{O^{2-},CaO} = n_{CaO}$	$N_1 = \frac{2n_1}{\sum n_i} = N_{CaO}$
	$Mn^{2+} + O^{2-}$	2	$n_2 = n_{Mn^{2+},MnO} = n_{O^{2-},MnO} = n_{MnO}$	$N_2 = \frac{2n_2}{\sum n_i} = N_{MnO}$
	$Mg^{2+} + O^{2-}$	3	$n_3 = n_{Mg^{2+},MgO} = n_{O^{2-},MgO} = n_{MgO}$	$N_3 = \frac{2n_3}{\sum n_i} = N_{MgO}$
	$Fe^{2+} + O^{2-}$	4	$n_4 = n_{Fe^{2+},FeO} = n_{O^{2-},FeO} = n_{FeO}$	$N_4 = \frac{2n_4}{\sum n_i} = N_{FeO}$
Simple molecules (3)	SiO_2	5	$n_5 = n_{SiO_2}$	$N_5 = \frac{n_5}{\sum n_i} = N_{SiO_2}$
	P_2O_5	6	$n_6 = n_{P_2O_5}$	$N_6 = \frac{n_6}{\sum n_i} = N_{P_2O_5}$
	Al_2O_3	7	$n_7 = n_{Al_2O_3}$	$N_7 = \frac{n_7}{\sum n_i} = N_{Al_2}O_3$
Complex molecules (32)	$CaO{\cdot}SiO_2$	c1	$n_{c1} = n_{CaO} \cdot SiO_2$	$N_{c1} = \frac{n_{c1}}{\sum n_i} = N_{CaO} \cdot SiO_2$
	$2CaO{\cdot}SiO_2$	c2	$n_{c2} = n_{2CaO} \cdot SiO_2$	$N_{c2} = \frac{n_{c2}}{\sum n_i} = N_{2CaO} \cdot SiO_2$
	$3CaO{\cdot}SiO_2$	c3	$n_{c3} = n_{3CaO} \cdot SiO_2$	$N_{c3} = \frac{n_{c3}}{\sum n_i} = N_{3CaO} \cdot SiO_2$
	$3CaO{\cdot}2SiO_2$	c4	$n_{c4} = n_{3CaO{\cdot}2SiO_2}$	$N_{c4} = \frac{n_{c4}}{\sum n_i} = N_{3CaO{\cdot}2SiO_2}$
	$3CaO{\cdot}Al_2O_3$	c5	$n_{c5} = n_{3CaO{\cdot}Al_2O_3}$	$N_{c5} = \frac{n_{c5}}{\sum n_i} = N_{3CaO{\cdot}Al_2O_3}$
	$CaO{\cdot}Al_2O_3$	c6	$n_{c6} = n_{CaO{\cdot}Al_2O_3}$	$N_{c6} = \frac{n_{c6}}{\sum n_i} = N_{CaO{\cdot}Al_2O_3}$
	$CaO{\cdot}2Al_2O_3$	c7	$n_{c7} = n_{CaO{\cdot}2Al_2O_3}$	$N_{c7} = \frac{n_{c7}}{\sum n_i} = N_{CaO{\cdot}2Al_2O_3}$
	$CaO{\cdot}6Al_2O_3$	c8	$n_{c8} = n_{CaO{\cdot}6Al_2O_3}$	$N_{c8} = \frac{n_{c8}}{\sum n_i} = N_{CaO{\cdot}6Al_2O_3}$
	$12CaO{\cdot}7Al_2O_3$	c9	$n_{c9} = n_{12CaO{\cdot}7Al_2O_3}$	$N_{c9} = \frac{n_{c9}}{\sum n_i} = N_{12CaO{\cdot}7Al_2O_3}$
	$MgO{\cdot}SiO_2$	c10	$n_{c10} = n_{MgO{\cdot}SiO_2}$	$N_{c10} = \frac{n_{c10}}{\sum n_i} = N_{MgO{\cdot}SiO_2}$
	$2MgO{\cdot}SiO_2$	c11	$n_{c11} = n_{2MgO{\cdot}SiO_2}$	$N_{c11} = \frac{n_{c11}}{\sum n_i} = N_{2MgO{\cdot}SiO_2}$
	$MgO{\cdot}Al_2O_3$	c12	$n_{c12} = n_{MgO{\cdot}Al_2O_3}$	$N_{c12} = \frac{n_{c12}}{\sum n_i} = N_{MgO{\cdot}Al_2O_3}$
	$2FeO{\cdot}SiO_2$	c13	$n_{c13} = n_{2FeO{\cdot}SiO_2}$	$N_{c13} = \frac{n_{c13}}{\sum n_i} = N_{2FeO{\cdot}SiO_2}$
	$FeO{\cdot}Al_2O_3$	c14	$n_{c14} = n_{FeO{\cdot}Al_2O_3}$	$N_{c14} = \frac{n_{c14}}{\sum n_i} = N_{FeO{\cdot}Al_2O_3}$
	$2MnO{\cdot}SiO_2$	c15	$n_{c15} = n_{2MnO{\cdot}SiO_2}$	$N_{c15} = \frac{n_{c15}}{\sum n_i} = N_{2MnO{\cdot}SiO_2}$
	$MnO{\cdot}SiO_2$	c16	$n_{c16} = n_{MnO{\cdot}SiO_2}$	$N_{c16} = \frac{n_{c16}}{\sum n_i} = N_{MnO{\cdot}SiO_2}$
	$MnO{\cdot}Al_2O_3$	c17	$n_{c17} = n_{MnO{\cdot}Al_2O_3}$	$N_{c17} = \frac{n_{c17}}{\sum n_i} = N_{MnO{\cdot}Al_2O_3}$
	$3Al_2O_3{\cdot}2SiO_2$	c18	$n_{c18} = n_{3Al_2O_3{\cdot}2SiO_2}$	$N_{c18} = \frac{n_{c18}}{\sum n_i} = N_{3Al_2O_3{\cdot}2SiO_2}$
	$2CaO{\cdot}SiO_2{\cdot}Al_2O_3$	c19	$n_{c19} = n_{2CaO{\cdot}SiO_2{\cdot}Al_2O_3}$	$N_{c19} = \frac{n_{c19}}{\sum n_i} = N_{2CaO{\cdot}SiO_2{\cdot}Al_2O_3}$
	$CaO{\cdot}2SiO_2{\cdot}Al_2O_3$	c20	$n_{c20} = n_{CaO{\cdot}2SiO_2{\cdot}Al_2O_3}$	$N_{c20} = \frac{n_{c20}}{\sum n_i} = N_{CaO{\cdot}2SiO_2{\cdot}Al_2O_3}$
	$CaO{\cdot}MgO{\cdot}SiO_2$	c21	$n_{c21} = n_{CaO{\cdot}MgO{\cdot}SiO_2}$	$N_{c21} = \frac{n_{c21}}{\sum n_i} = N_{CaO{\cdot}MgO{\cdot}SiO_2}$
	$CaO{\cdot}MgO{\cdot}2SiO_2$	c22	$n_{c22} = n_{CaO{\cdot}MgO{\cdot}2SiO_2}$	$N_{c22} = \frac{n_{c22}}{\sum n_i} = N_{CaO{\cdot}MgO{\cdot}2SiO_2}$
	$2CaO{\cdot}MgO{\cdot}2SiO_2$	c23	$n_{c23} = n_{2CaO{\cdot}MgO{\cdot}2SiO_2}$	$N_{c23} = \frac{n_{c23}}{\sum n_i} = N_{2CaO{\cdot}MgO{\cdot}2SiO_2}$
	$3CaO{\cdot}MgO{\cdot}2SiO_2$	c24	$n_{c24} = n_{3CaO{\cdot}MgO{\cdot}2SiO_2}$	$N_{c24} = \frac{n_{c24}}{\sum n_i} = N_{3CaO{\cdot}MgO{\cdot}2SiO_2}$
	$2MgO{\cdot}5SiO_2{\cdot}2Al_2O_3$	c25	$n_{c25} = n_{2MgO{\cdot}5SiO_2{\cdot}2Al_2O_3}$	$N_{c25} = \frac{n_{c25}}{\sum n_i} = N_{2MgO{\cdot}5SiO_2{\cdot}2Al_2O_3}$
	$2CaO{\cdot}P_2O_5$	c26	$n_{c26} = n_{2CaO{\cdot}P_2O_5}$	$N_{c26} = \frac{n_{c26}}{\sum n_i} = N_{2CaO{\cdot}P_2O_5}$
	$3CaO{\cdot}P_2O_5$	c27	$n_{c27} = n_{3CaO{\cdot}P_2O_5}$	$N_{c27} = \frac{n_{c27}}{\sum n_i} = N_{3CaO{\cdot}P_2O_5}$
	$4CaO{\cdot}P_2O_5$	c28	$n_{c28} = n_{4CaO{\cdot}P_2O_5}$	$N_{c28} = \frac{n_{c28}}{\sum n_i} = N_{4CaO{\cdot}P_2O_5}$
	$3FeO{\cdot}P_2O_5$	c29	$n_{c29} = n_{3FeO{\cdot}P_2O_5}$	$N_{c29} = \frac{n_{c29}}{\sum n_i} = N_{3FeO{\cdot}P_2O_5}$
	$4FeO{\cdot}P_2O_5$	c30	$n_{c30} = n_{4FeO{\cdot}P_2O_5}$	$N_{c30} = \frac{n_{c30}}{\sum n_i} = N_{4FeO{\cdot}P_2O_5}$
	$2MgO{\cdot}P_2O_5$	c31	$n_{c31} = n_{2MgO{\cdot}P_2O_5}$	$N_{c31} = \frac{n_{c31}}{\sum n_i} = N_{2MgO{\cdot}P_2O_5}$
	$3MgO{\cdot}P_2O_5$	c32	$n_{c32} = n_{3MgO{\cdot}P_2O_5}$	$N_{c32} = \frac{n_{c32}}{\sum n_i} = N_{3MgO{\cdot}P_2O_5}$

$$N_1 + N_2 + N_3 + N_4 + N_5 + N_6 + N_7 + N_{c1} + N_{c2} + N_{c3} + N_{c4} + \cdots + N_{c30} + N_{c31} + N_{c32} = (N_1 + N_2 + N_3 + N_4 + N_5 + N_6 + N_7 + K_{c1}^{\Theta} N_1 N_5 + K_{c2}^{\Theta} N_1^2 N_5 + K_{c3}^{\Theta} N_1^3 N_5 + K_{c4}^{\Theta} N_1^3 N_5^2 + \cdots + K_{c30}^{\Theta} N_4^4 N_6 + K_{c31}^{\Theta} N_3^2 N_6 + K_{c32}^{\Theta} N_3^3 N_6) = \sum N_i = 1.0 \quad [12]$$

Eqs. Eqs. [5] through [12] are the governing equations for calculating the mass action concentration N_i of structural units or ion couples in the dephosphorization slag of CaO-FeO-SiO_2-MgO-MnO-Al_2O_3-P_2O_5. According to Eqs. [5] through [12], there are eight unknown parameters of N_1, N_2, N_3, N_4, N_5, N_6, N_7 and $\sum n_i$, combined with the eight independent governing equations built by IMCT. The mass action concentration N_i of simple components and the total equilibrium mole number $\sum n_i$ can be obtained, thus the mass action concentration N_{ci} of complex components can be calculated, and the reaction ability of complex components can be further studied. The solution of the Eqs. (5-12) can be obtained by Jupyter Notebook in Anaconda, and the accuracy of the solution of nonlinear equations by calling Fsolve Function can reach to be smaller than 10^{-25}. Therefore, it can be considered that the obtained N_i is very accurate.

D. *Definition of Enrichment Possibility N_{Ci-Pj}, Enrichment Degree R_{Ci-Pj} of Solid Solution Containing P_2O_5 and Phosphorus-Enrichment Contribution Ratio of Calcium Silicate R_{Ci}*

Senlin Xie *et al.*[27] and Jingyan Li *et al.*[28,29] both studied the enrichment behavior of phosphorus in calcium silicate based on IMCT. P_2O_5 is mainly concentrated in calcium silicate complex molecules, so the solid phase rich in P_2O_5 can be regarded as the reaction product of calcium silicate and phosphate, independent of other structural units.[27] There are four kinds of calcium silicate molecules and seven kinds of phosphate in the dephosphorization slag in the present work. Therefore, the product of mass action concentration N_{Ci} of calcium silicate and N_{Pj} of containing P_2O_5 component can be used to describe the enrichment possibility N_{Ci-Pj} of solid solution containing P_2O_5 in dephosphorization slag,[27–29] as shown in Eq. [13]:

$$N_{Ci-Pj} = N_{Ci} \times N_{Pj} \text{ with } i = 1,2,3,4,\ j = 1,2,3,4,5,6,7 \quad [13]$$

Ci includes CS, C_2S, C_3S, $3CaO{\cdot}2SiO_2(C_3S_2)$.

Pj includes $2CaO{\cdot}P_2O_5(C_2P)$, $3CaO{\cdot}P_2O_5(C_3P)$, $4CaO{\cdot}P_2O_5(C_4P)$, $3FeO{\cdot}P_2O_5(F_3P)$, $4FeO{\cdot}P_2O_5(F_4P)$, $2MgO{\cdot}P_2O_5(M_2P)$, $3MgO{\cdot}P_2O_5(M_3P)$.

The sum of the enrichment possibility N_{Ci-Pj} of the above-mentioned twenty-eight components containing P_2O_5 components is expressed by Eq. [14]:

$$\sum_{\substack{i=1,2,3,4 \\ j=1,2,3,4,5,6,7}} \left(N_{Ci-Pj} \frac{M_{P_2O_5}}{M_{Ci-Pj}} \right) = N_{C1-P1} \frac{M_{P_2O_5}}{M_{C1-P1}} + N_{C1-P2} \frac{M_{P_2O_5}}{M_{C1-P2}} + \ldots + N_{C4-P7} \frac{M_{P_2O_5}}{M_{C4-P7}} \quad [14]$$

M_i is the relative atomic or molecular mass of i. The ratio of $N_{Ci-Pj} \frac{M_{P_2O_5}}{M_{Ci-Pj}}$ of a certain components to the sum of the enrichment possibility for all the components containing P_2O_5, $\sum_{\substack{i=1,2,3,4 \\ j=1,2,34,5,6,7}} \left(N_{Ci-Pj} \frac{M_{P_2O_5}}{M_{Ci-Pj}} \right)$, can be defined as the enrichment degree R_{Ci-Pj} of solid solution containing P_2O_5.[27–29] Taking C_2S-C_3P as an example, the enrichment degree $R_{C2S-C3P}$ is expressed as Eq. [15]:

$$R_{C2S-C3P} = \frac{\left(N_{C2S-C3P} \frac{M_{P2O5}}{M_{C2S-C3P}} \right)}{\sum_{\substack{i=1,2,3,4 \\ j=1,2,3,4,5,6,7}} \left(N_{Ci-Pj} \frac{M_{P2O5}}{M_{Ci-Pj}} \right)} \quad [15]$$

In order to describe the phosphorus-enrichment capacity of a certain calcium silicate in the dephosphorization slag, the sum of the enrichment degree R_{Ci-Pj} of all components containing P_2O_5 in a certain calcium silicate is defined as the phosphorus-enrichment contribution ratio R_{Ci} of calcium silicate.[27] Taking C_2S as an example, the phosphorus-enrichment contribution ratio R_{C2S} can be expressed as Eq. [16]:

$$R_{C2S} = R_{C2S-C2P} + R_{C2S-C3P} + \ldots + R_{C2S-M3P} = \frac{\sum_{\substack{i=2 \\ j=1,2,3,4,5,6,7}} \left(N_{C2S-Pj} \frac{M_{P2O5}}{M_{C2S-Pj}} \right)}{\sum_{\substack{i=1,2,3,4 \\ j=1,2,3,4,5,6,7}} \left(N_{Ci-Pj} \frac{M_{P2O5}}{M_{Ci-Pj}} \right)} \quad [16]$$

IV. ANALYSIS AND DISCUSSION OF HOT METAL SAMPLES AND DEPHOSPHORIZATION SLAG SAMPLES FROM INDUSTRIAL EXPERIMENTS

A. *Effect of Dephosphorization Slag Basicity on Element Removal Ratio in Hot Metal, Phosphorus Distribution Ratio Between Slag and Hot Metal*

In industrial experiment, it is difficult to control all the other parameters to be constants for investigating the effect of dephosphorization slag basicity on hot metal dephosphorization. In the heats of industrial

Table VI. Chemical Reaction of Formed Complex Molecules in the Dephosphorization Slag of CaO-FeO-SiO_2-MgO-MnO-Al_2O_3-P_2O_5, Their Standerd Molar Gibbs Free Energy $\Delta_r G^{\Theta}_{m,ci}$ Changed With T, Standard Equilibrium Constant K^{Θ}_{ci} and Complex Molecular Mass Action Concentration N_{ci} Expressed by N_1-N_7 and Equilibrium Constant K^{Θ}_{ci}

Reactions	$\Delta_r G^{\Theta}_{m,ci}$	K^{Θ}_{ci}	N_{ci}
$(Ca^{2+}+O^{2-})+(SiO_2)=(CaO\cdot SiO_2)$	$-21757-36.819T$[22]	$K^{\Theta}_{c1}=\frac{N_{c1}}{N_1N_5}$	$N_{c1}=K^{\Theta}_{c1}N_1N_5$
$2(Ca^{2+}+O^{2-})+(SiO_2)=(2CaO\cdot SiO_2)$	$-102090-24.267T$[22]	$K^{\Theta}_{c2}=\frac{N_{c2}}{N_1^2N_5}$	$N_{c2}=K^{\Theta}_{c2}N_1^2N_5$
$3(Ca^{2+}+O^{2-})+(SiO_2)=(3CaO\cdot SiO_2)$	$-118826-6.694T$[22]	$K^{\Theta}_{c3}=\frac{N_{c3}}{N_1^3N_5}$	$N_{c3}=K^{\Theta}_{c3}N_1^3N_5$
$3(Ca^{2+}+O^{2-})+2(SiO_2)=(3CaO\cdot 2SiO_2)$	$-236973+9.63T$[27]	$K^{\Theta}_{c4}=\frac{N_{c4}}{N_1^3N_5^2}$	$N_{c4}=K^{\Theta}_{c4}N_1^3N_5^2$
$3(Ca^{2+}+O^{2-})+(Al_2O_3)=(3CaO\cdot Al_2O_3)$	$-21757-29.288T$[22]	$K^{\Theta}_{c5}=\frac{N_{c5}}{N_1^3N_7}$	$N_{c5}=K^{\Theta}_{c5}N_1^3N_7$
$(Ca^{2+}+O^{2-})+(Al_2O_3)=(CaO\cdot Al_2O_3)$	$59413-59.413T$[25]	$K^{\Theta}_{c6}=\frac{N_{c6}}{N_1N_7}$	$N_{c6}=K^{\Theta}_{c6}N_1N_7$
$(Ca^{2+}+O^{2-})+2(Al_2O_3)=(CaO\cdot 2Al_2O_3)$	$-16736-25.522T$[25]	$K^{\Theta}_{c7}=\frac{N_{c7}}{N_1N_7^2}$	$N_{c7}=K^{\Theta}_{c7}N_1N_7^2$
$(Ca^{2+}+O^{2-})+6(Al_2O_3)=(CaO\cdot 6Al_2O_3)$	$-22594-31.798T$[25]	$K^{\Theta}_{c8}=\frac{N_{c8}}{N_1N_7^6}$	$N_{c8}=K^{\Theta}_{c8}N_1N_7^6$
$12(Ca^{2+}+O^{2-})+7(Al_2O_3)=(12CaO\cdot 7Al_2O_3)$	$617977-612.119T$[25]	$K^{\Theta}_{c9}=\frac{N_{c9}}{N_1^{12}N_7^7}$	$N_{c9}=K^{\Theta}_{c9}N_1^{12}N_7^7$
$(Mg^{2+}+O^{2-})+(SiO_2)=(MgO\cdot SiO_2)$	$23849-29.706T$[25]	$K^{\Theta}_{c10}=\frac{N_{c10}}{N_3N_5}$	$N_{c10}=K^{\Theta}_{c10}N_3N_5$
$2(Mg^{2+}+O^{2-})+(SiO_2)=(2MgO\cdot SiO_2)$	$-56902-3.347T$[25]	$K^{\Theta}_{c11}=\frac{N_{c11}}{N_3^2N_5}$	$N_{c11}=K^{\Theta}_{c11}N_3^2N_5$
$(Mg^{2+}+O^{2-})+(Al_2O_3)=(MgO\cdot Al_2O_3)$	$-18828-6.276T$[25]	$K^{\Theta}_{c12}=\frac{N_{c12}}{N_3N_7}$	$N_{c12}=K^{\Theta}_{c12}N_3N_7$
$2(Fe^{2+}+O^{2-})+(SiO_2)=(2FeO\cdot SiO_2)$	$-9395-0.227T$	$K^{\Theta}_{c13}=\frac{N_{c13}}{N_4^2N_5}$	$N_{c13}=K^{\Theta}_{c13}N_4^2N_5$
$(Fe^{2+}+O^{2-})+(Al_2O_3)=(FeO\cdot Al_2O_3)$	$-59204+22.343T$[25]	$K^{\Theta}_{c14}=\frac{N_{c14}}{N_4N_7}$	$N_{c14}=K^{\Theta}_{c14}N_4N_7$
$2(Mn^{2+}+O^{2-})+(SiO_2)=(2MnO\cdot SiO_2)$	$36066-30.669T$	$K^{\Theta}_{c15}=\frac{N_{c15}}{N_2^2N_5}$	$N_{c15}=K^{\Theta}_{c15}N_2^2N_5$
$(Mn^{2+}+O^{2-})+(SiO_2)=(MnO\cdot SiO_2)$	$38911-40.041T$[25]	$K^{\Theta}_{c16}=\frac{N_{c16}}{N_2N_5}$	$N_{c16}=K^{\Theta}_{c16}N_2N_5$
$(Mn^{2+}+O^{2-})+(Al_2O_3)=(MnO\cdot Al_2O_3)$	$-45116+11.81T$[25]	$K^{\Theta}_{c17}=\frac{N_{c17}}{N_2N_7}$	$N_{c17}=K^{\Theta}_{c17}N_2N_7$
$2(SiO_2)+3(Al_2O_3)=(2SiO_2\cdot 3Al_2O_3)$	$-4351-10.46T$[25]	$K^{\Theta}_{c18}=\frac{N_{c18}}{N_5^2N_7^3}$	$N_{c18}=K^{\Theta}_{c18}N_5^2N_7^3$
$2(Ca^{2+}+O^{2-})+(Al_2O_3)+(SiO_2)=(2CaO\cdot Al_2O_3\cdot SiO_2)$	$-116315-38.911T$[22]	$K^{\Theta}_{c19}=\frac{N_{c19}}{N_1^2N_5N_7}$	$N_{c19}=K^{\Theta}_{c19}N_1^2N_5N_7$
$(Ca^{2+}+O^{2-})+(Al_2O_3)+2(SiO_2)=(CaO\cdot Al_2O_3\cdot 2SiO_2)$	$-4184-73.638T$[22]	$K^{\Theta}_{c20}=\frac{N_{c20}}{N_1N_5^2N_7}$	$N_{c20}=K^{\Theta}_{c20}N_1N_5^2N_7$
$(Ca^{2+}+O^{2-})+(Mg^{2+}+O^{2-})+(SiO_2)=(CaO\cdot MgO\cdot SiO_2)$	$-124683+3.766T$[22]	$K^{\Theta}_{c21}=\frac{N_{c21}}{N_1N_3N_5}$	$N_{c21}=K^{\Theta}_{c21}N_1N_3N_5$
$(Ca^{2+}+O^{2-})+(Mg^{2+}+O^{2-})+2(SiO_2)=(CaO\cdot MgO\cdot 2SiO_2)$	$-80333-51.882T$[22]	$K^{\Theta}_{c22}=\frac{N_{c22}}{N_1N_3N_5^2}$	$N_{c22}=K^{\Theta}_{c22}N_1N_3N_5^2$
$2(Ca^{2+}+O^{2-})+(Mg^{2+}+O^{2-})+2(SiO_2)=(2CaO\cdot MgO\cdot 2SiO_2)$	$-73638-63.597T$[22]	$K^{\Theta}_{c23}=\frac{N_{c23}}{N_1^2N_3N_5^2}$	$N_{c23}=K^{\Theta}_{c23}N_1^2N_3N_5^2$
$3(Ca^{2+}+O^{2-})+(Mg^{2+}+O^{2-})+2(SiO_2)=(3CaO\cdot MgO\cdot 2SiO_2)$	$-205016-31.798T$[22]	$K^{\Theta}_{c24}=\frac{N_{c24}}{N_1^3N_3N_5^2}$	$N_{c24}=K^{\Theta}_{c24}N_1^3N_3N_5^2$

Table VI. continued

Reactions	$\Delta_r G^{\Theta}_{m,ci}$	K^{Θ}_{ci}	N_{ci}
$2(Mg^{2+} + O^{2-}) + 5(SiO_2) + 2(Al_2O_3) = (2MgO \cdot 5SiO_2 \cdot 2Al_2O_3)$	$-14422 - 14.808T$ [22]	$K^{\Theta}_{c25} = \frac{N_{c25}}{N_3^2 N_5^5 N_7^2}$	$N_{c25} = K^{\Theta}_{c25} N_3^2 N_5^5 N_7^2$
$2(Ca^{2+} + O^{2-}) + (P_2O_5) = (2CaO \cdot P_2O_5)$	$-484372 - 26.569T$ [25]	$K^{\Theta}_{c26} = \frac{N_{c26}}{N_1^2 N_6}$	$N_{c26} = K^{\Theta}_{c26} N_1^2 N_6$
$3(Ca^{2+} + O^{2-}) + (P_2O_5) = (3CaO \cdot P_2O_5)$	$-709890 + 6.150T$ [25]	$K^{\Theta}_{c27} = \frac{N_{c27}}{N_1^3 N_6}$	$N_{c27} = K^{\Theta}_{c27} N_1^3 N_6$
$4(Ca^{2+} + O^{2-}) + (P_2O_5) = (4CaO \cdot P_2O_5)$	$-661356 - 3.473T$ [25]	$K^{\Theta}_{c28} = \frac{N_{c28}}{N_1^4 N_6}$	$N_{c28} = K^{\Theta}_{c28} N_1^4 N_6$
$3(Fe^{2+} + O^{2-}) + (P_2O_5) = (3FeO \cdot P_2O_5)$	$-430404 + 92.708T$ [25]	$K^{\Theta}_{c29} = \frac{N_{c29}}{N_4^3 N_6}$	$N_{c29} = K^{\Theta}_{c29} N_4^3 N_6$
$4(Fe^{2+} + O^{2-}) + (P_2O_5) = (4FeO \cdot P_2O_5)$	$-512251 + 128.083T$ [25]	$K^{\Theta}_{c30} = \frac{N_{c30}}{N_4^4 N_6}$	$N_{c30} = K^{\Theta}_{c30} N_4^4 N_6$
$2(Mg^{2+} + O^{2-}) + (P_2O_5) = (2MgO \cdot P_2O_5)$	$168369 - 339.357T$ [25]	$K^{\Theta}_{c31} = \frac{N_{c31}}{N_3^2 N_6}$	$N_{c31} = K^{\Theta}_{c31} N_3^2 N_6$
$3(Mg^{2+} + O^{2-}) + (P_2O_5) = (3MgO \cdot P_2O_5)$	-267641 to $115.186T$ [25]	$K^{\Theta}_{c32} = \frac{N_{c32}}{N_3^3 N_6}$	$N_{c32} = K^{\Theta}_{c32} N_3^3 N_6$

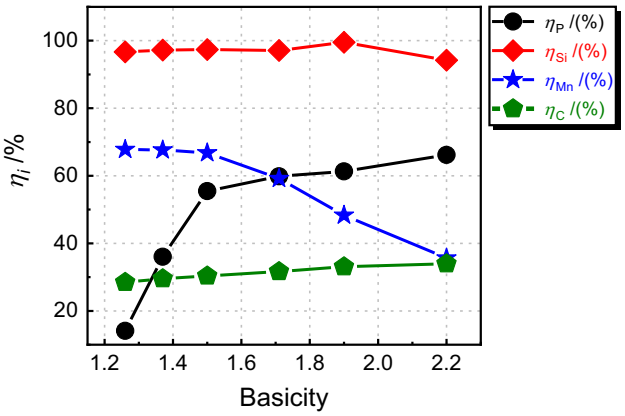

Fig. 3—Effect of dephosphorization slag basicity on removal ratios of elements in hot metal.

experiments selected in the present work, the dephosphorization endpoint temperatures were 1370 °C to 1420 °C. From the previous industrial experiment results,[5,9,30,31] the slagging effect of dephosphorization slag was favorable in this temperature range, and the thermodynamic conditions were conducive to dephosphorization. The FeO contents changed in a narrow range of 17.04 to 20.48 pct, which ensured a relatively close oxidation capacity. The contents of MgO, MnO and Al_2O_3 changed little, and these changes did not have a great impact on the dephosphorization results. The changes in the removal ratios of phosphorus, silicon, carbon and manganese in hot metal, phosphorus distribution ratio between dephosphorization slag and hot metal at the different dephosphorization slag basicities from 1.26 to 2.20 were studied.

Figure 3 shows the effect of dephosphorization slag basicity on removal ratios of elements in hot metal. η_i is the removal ratio of element i in hot metal, which is calculated by Eq. [17]. [pct i]$_0$ represents the mass fraction of i in the hot metal at the initial point of dephosphorization and [pct i]$_e$ represents that at the endpoint of dephosphorization. The chemical reactions of dephosphorization, desilication, demanganization and decarbonization in hot metal are expressed as Eqs. [18] through [21].[32–36]

$$\eta_i = \frac{[\text{pct } i]_0 - [\text{pct } i]_e}{[\text{pct } i]_0} \times 100 \text{ pct} \quad [17]$$

$$2[P] + 5(FeO) + 3CaO = (3CaO \cdot P_2O_5) + 5[Fe] \quad [18]$$

$$[Si] + 2(FeO) = (SiO_2) + 2[Fe] \quad [19]$$

$$[Mn] + (FeO) = (MnO) + [Fe] \quad [20]$$

$$[C] + [O] = CO \quad [21]$$

It can be seen from Figure 3 that with increasing dephosphorization slag basicity, the dephosphorization ratio and the decarbonization ratio both increases, and the demanganization ratio gradually decreases, while the desiliconization ratio does not change significantly and remains at a relatively high level. With increasing dephosphorization slag basicity, the activity of CaO in slag increases, and the calcium silicate is easier to form in the slag, which is conducive to the formation of C_2S-C_3P solid solution. According to the chemical reaction of Eq. [18], increasing the dephosphorization slag basicity is beneficial to reduce the activity of P_2O_5 in the slag, so as to improve the phosphorus distribution ratio between slag and hot metal, and further improve the dephosphorization ratio.

With increasing dephosphorization slag basicity, the oxygen potential at the interface between slag and hot metal is increased, and the decarburization reaction is also promoted. However, the decarburization reaction is weak in the dephosphorization stage, and the decarburization ratio is from 28.46 to 33.95 pct. In the dephosphorization stage, the combination ability of silicon and manganese with oxygen is stronger than that of phosphorus, so that silicon and manganese will be oxidized prior to phosphorus. With increasing dephosphorization slag basicity, the activity of SiO_2 in the slag decreases, which is conducive to the desilication reaction. The desilication ratio at the end of dephosphorization is always above 94 pct, so that silicon in hot metal is removed to trace at the end of dephosphorization stage. The increase of basicity leads to the existence of a large amount of free CaO in the dephosphorization slag. CaO will replace the MnO in $2MnO{\cdot}SiO_2$ to generate the stabler C_2S,[36] thus increasing the activity of MnO. This will lead to the occurrence of remanganization reaction, reducing the demanganization ratio. When the dephosphorization slag basicity is 2.20, the dephosphorization ratio can reach 66.20 pct. The desilication ratio, demanganization ratio and the decarburization ratio are 94.22, 35.65 and 33.95 pct, respectively.

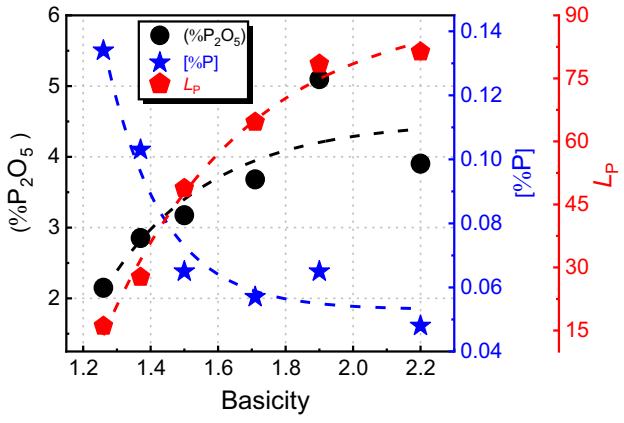

Fig. 4—Effect of dephosphorization slag basicity on P_2O_5 content in dephosphorization slag, phosphorus content in hot metal and phosphorus distribution ratio L_P.

Figure 4 shows the effect of dephosphorization slag basicity on P_2O_5 content in dephosphorization slag, phosphorus content in hot metal and phosphorus distribution ratio L_P. Phosphorus distribution ratio L_P is calculated by Eq. [22].

$$L_P = \frac{(\text{pct } P_2O_5)}{[\text{pct P}]} \quad [22]$$

With increasing the dephosphorization slag basicity, the phosphorus distribution ratio L_P increases, the content of P_2O_5 in dephosphorization slag increases as a whole and the phosphorus content in hot metal decreases. When the dephosphorization slag basicity is 1.90, the P_2O_5 content in the slag can reach 5.10 pct. When the dephosphorization slag basicity is further increased to 2.20, the phosphorus distribution ratio increases to 81.3 and the phosphorus content in hot metal decreases to 0.048 pct. The increase of dephosphorization slag basicity improves the apparent diffusion coefficient of phosphorus in solid solution,[37] which makes the phosphorus in hot metal more easily fixed in C_2S-C_3P solid solution. This increases the content of P_2O_5 in slag and reduces the phosphorus content in hot metal.

B. *XRD Analysis of Dephosphorization Slag Under Different Basicities*

Figure 5 shows the XRD analysis results of dephosphorization slag with basicities of 1.26 to 2.20. At the endpoint of the dephosphorization stage in the NDSP, the dephosphorization slag mainly contains dicalcium silicate $Ca_2SiO_4(C_2S)$, silicate phase $Ca_3Mg(SiO_4)_2$, calcium ferrite phase $Ca_2Fe_2O_5$, the $Ca(Fe_xMg_y)(SiO_4)(x+y=1)$ mixture of $Ca_3Mg(SiO_4)_2$ and $Ca_2Fe_2O_5$, metal oxide phase RO and the solid solution of $(Ca_2(SiO_4))6(Ca_3(PO_4)_2)(C_2S\text{-}6C_3P)$ and $Ca_{15}(PO_4)_2(SiO_4)_6(6C_2S\text{-}C_3P)$ containing phosphorus.

By comparing the XRD results of dephosphorization slags with different basicites, it is found that the mixed phase of $Ca(Fe_xMg_y)(SiO_4)(x + y = 1)$ is widely existed in dephosphorization slag when basicity is 1.26 to 1.37, and there is no oxide phase and the solid solution phase containing phosphorus. Combined with the dephosphorization results in Figure 3 and our previous mineralogical analysis[9] of the dephosphorization slag under low basicity, a reasonable explanation can be obtained. Because there is a large amount of liquid slag matrix phase in the slag at lower basicity, phosphorus in hot metal is difficult to be effectively fixed in dephosphorization slag. Large-area P-rich phase in the dephosphorization slag is hard to form, which leads to the low dephosphorization ratio at lower basicity.

When the basicity range of dephosphorization slag is 1.37 to 1.71, C_2S, $Ca_3Mg(SiO_4)_2$, $Ca_2Fe_2O_5$ and RO are mainly detected in the dephosphorization slag, which indicates that the dephosphorization slag changes from liquid slag matrix phase to silicate and calcium ferrite. However, the solid solution containing phosphorus has not been detected by XRD in this range. When the basicity range of dephosphorization slag is further

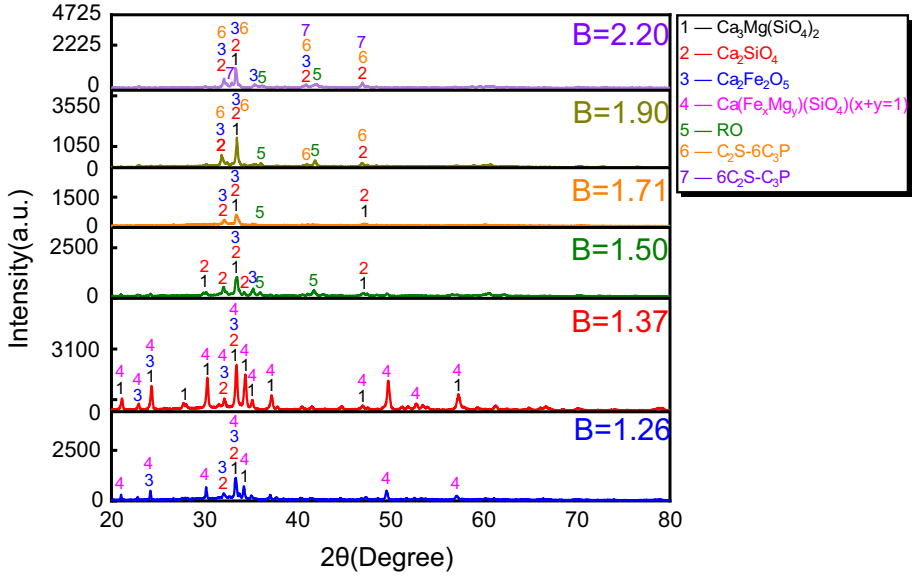

Fig. 5—XRD analysis results of dephosphorization slag with basicities of 1.26 to 2.20.

increased to 1.90 to 2.20, the diffraction peaks of C_2S-$6C_3P$ and $6C_2S$-C_3P phases appear, which is consistent with the higher dephosphorization ratio as shown in Figure 3.

C. *Analysis of P-Rich Phase Morphologies and Areas in Dephosphorization Slag at Different Basicities by SEM-EDS*

The typical morphologies, areas and map scanning results of P-rich phase in dephosphorization slag at different basicities are shown in Figure 6. When the dephosphorization slag basicity is in the range of 1.26 to 1.37, the P-rich phases are in long strip shape, and their area is between 4 and 36 μm^2. The content of P_2O_5 in the P-rich phase is less than 10 pct and it contains high contents of Ca and Si. The map scanning result is not obvious for the identification of phosphorus element in each phase. Therefore, it is inferred that the solid solution containing phosphorus is not formed in the basicity range of 1.26 to 1.37.

When the dephosphorization slag basicity is 1.50, the P-rich phases are dispersed into several small block P-rich phases, which are mainly distributed in dendrite shape, and their areas are mainly concentrated in 8 to 25 μm^2. When the dephosphorization slag basicity is further increased to the range of 1.71 to 2.20, the dispersed small block P-rich phase grows rapidly, irregular blocks gradually grow into the blocks with smooth edge, and the area of P-rich phase grows from 142 μm^2 at basicity of 1.71 to 8000 μm^2 at the basicity of 2.20. It can be seen from Figure 6 that the Ca, Si and P are mainly concentrated in the P-rich phase. Therefore, according to the results of Figures 5 and 6, the solid solution containing phosphorus is formed in the basicity range of 1.90 to 2.20.

D. *Analysis of P-Rich Phase at Different Basicities*

In order to determine the existing form of phosphorus containing solid solution (C_iS-C_jP) in P-rich phase of dephosphorization slag, five groups of P-rich phase composition data were obtained by SEM-EDS analysis under each basicity, and the results were averaged to reduce the element content differences caused by different points in the P-rich phase. Because phosphorus mainly exists in the form of C_3P in the solid solution,[16,17] and the sum of the masses of CaO, SiO_2 and P_2O_5 in the P-rich phase is equal to the sum of C_iS and C_3P, the average mass fraction of C_iS and C_3P can be calculated. According to the mass fraction ratio of CaO and SiO_2 in the P-rich phase, it can be seen that the calcium silicate existing in the P-rich phase is mainly the mixture of CS and C_2S. Table VII shows the average mass fractions of different compositions in P-rich phase of dephosphorization slag and the average mass fractions of C_3P and C_iS at the different basicities.

Figure 7(a) shows the Gibbs free energy changes of C_iS($i=1$, 2) and C_jP($j=1,2,3$) under different basicities of dephosphorization slag, Figure 7(b) shows the effect of dephosphorization slag basicity on C_3P content, basicity, C_iS content in P-rich phase of dephosphorization slag and Figure 7(c) shows the determination of coefficient n in nC_2S-C_3P of the P-rich phase at different basicities. The Gibbs free energy of each substance in Figure 7(a) is calculated according to Table VI. With increasing dephosphorization slag basicity, the content of C_3P and basicity of P-rich phase increase, the content of C_iS decreases as a whole. The basicity in P-rich phase increases from 1.21 to 1.97, which corresponds to the actual basicity change of dephosphorization slag. It also shows that calcium silicate in P-rich phase is a mixture of CS and C_2S. By comparing the free energy of

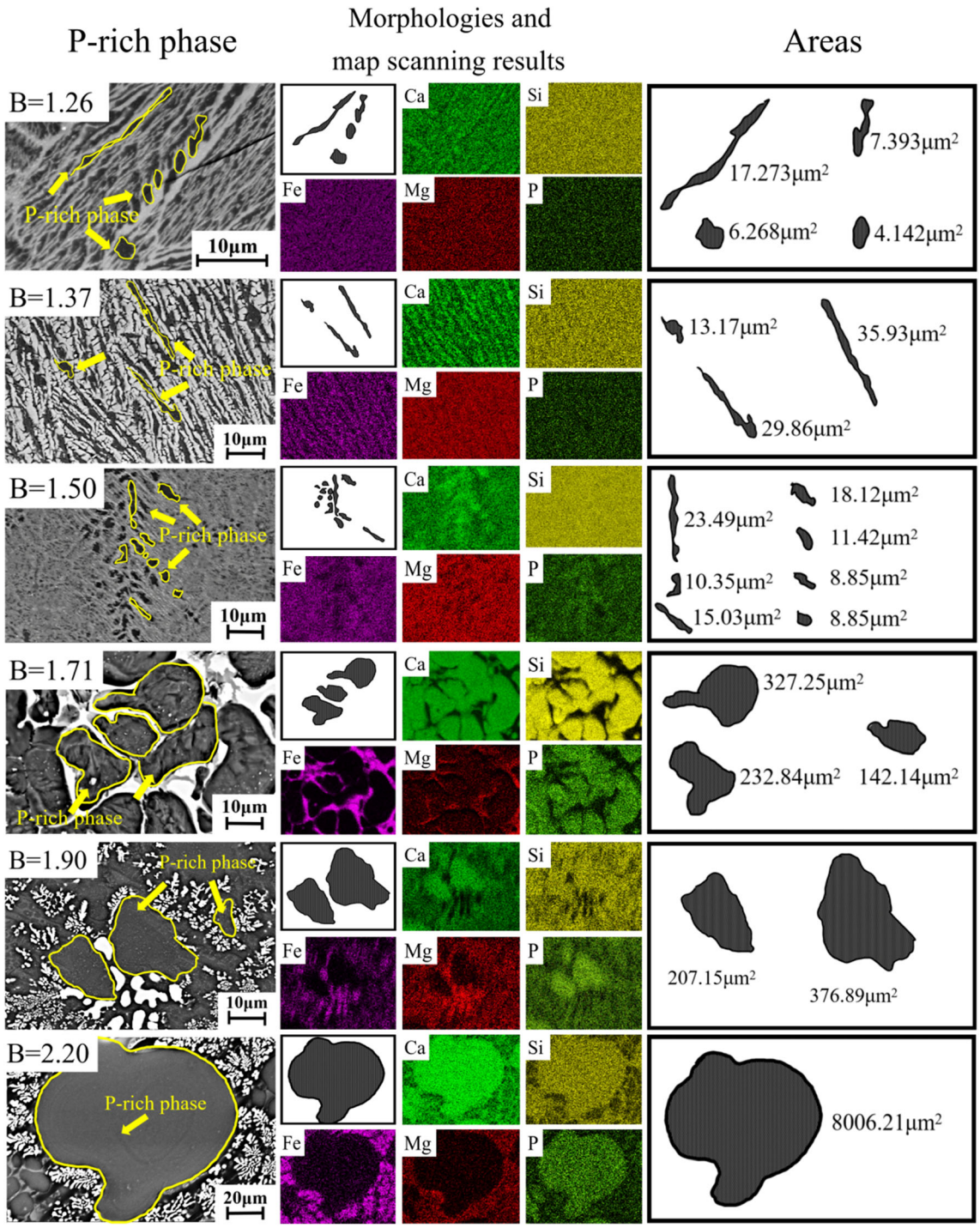

Fig. 6—Typical morphologies, areas and map scanning results of P-rich phase in dephosphorization slag at different basicities.

formation of $C_iS(i = 1, 2)$ and $C_jP(j = 1,2,3)$ at different basicities, C_iS is stabler than C_jP at 1370 °C to 1420 °C, and the combination ability of CaO with P_2O_5 is stronger than that with SiO_2.[38–40] With the increase of P_2O_5 content in the P-rich phase, CaO will first combine with P_2O_5 to form C_3P. Therefore, with increasing dephosphorization slag basicity, the content of C_3P increases and the content of C_iS decreases in P-rich phase.

The phosphorus containing solid solution in dephosphorization slag may exist in the form of C_2S-C_3P, $2C_2S$-C_3P, $4.8C_2S$-C_3P, $6C_2S$-C_3P and $20C_2S$-C_3P.[30] Therefore, taking nC_2S-C_3P (n = 1, 2, 4.8, 6, 20) as the judgment standard, the coefficient n in nC_2S-C_3P of P-rich phase under different basicities is roughly determined, as shown in Figure 7(c). When the dephosphorization slag basicity is 1.26 to 1.37, the values of n are 6 to 20. When the basicity is 1.50 to 1.90, the values of n

are 2 to 4.8. When the basicity further increases to 2.20, the values of n are 1 to 2. The results show that with increasing the basicity, the coefficient n of $n$$C_2S$-$C_3P$ presents a decreasing trend, which indicates that the phosphorus content in $n$$C_2S$-$C_3P$ increases gradually with increasing basicity, and the phosphorus-enrichment ability of the dephosphorization slag increases.

V. ANALYSIS AND DISCUSSION OF IMCT THERMODYNAMIC CALCUATION RESULTS

A. *Effect of Dephosphorization Slag Basicity on Mass Action Concentration N_i of Components in Dephosphorization Slag*

According to the IMCT-N_i thermodynamic calculation model, the mass action concentration N_i of each component in Table VI was calculated. The mass action concentration N_i in IMCT can be used to characterize the reaction capacity of the composition like the activity a_i in molecular theory.[18–21,25] In order to study the relationship between mass action concentration N_i and the basicity of dephosphorization slag, the best fitting method was selected according to the data changing rule, and the goodness of fit was expressed by the fitting coefficient r^2.

In order to analyze the phosphorus-enrichment capacity of calcium silicate in dephosphorization slag, the effect of dephosphorization slag basicity on mass action concentration of CaO , SiO_2 and the their ratio are analyzed. Figure 8 shows the effect of dephosphorization slag basicity on N_{CaO}, N_{SiO_2} and N_{CaO}/N_{SiO_2}. With increasing dephosphorization slag basicity, N_{CaO} increases exponentially and N_{SiO_2} decreases exponentially. The fitting coefficient r^2 of both is greater than 0.97, which indicates that there is a good mathematical relationship between the dephosphorization slag basicity and N_{CaO} and N_{SiO_2}.

With increasing dephosphorization slag basicity, N_{CaO}/N_{SiO_2} increases exponentially, and its fitting coefficient is greater than 0.999, reaching the fitting convergence. The results show that both basicities of B and N_{CaO}/N_{SiO_2} have the similar effect in dephosphorization slag at temperature of 1370 °C to 1420 °C and basicity of 1.26 to 2.20. The relationship between B and N_{CaO}/N_{SiO_2} is Eq. [23]. It should be noted that the range of N_{CaO}/N_{SiO_2} has large values of 4 to 1202, so that Eq. [23] can only reflect the their change trends.

$$N_{CaO}/N_{SiO_2} = 6.774 \times 10^{-5} \times \exp\left(\frac{B}{0.1403}\right) + 5.674 \quad [23]$$

Four kinds of calcium silicate complex molecules CS, C_2S, C_3S, C_3S_2 formed by CaO and SiO_2 are further considered. The effect of dephosphorization slag basicity on the mass action concentration of calcium silicates were analyzed under the conditions of lower temperature range of 1370 °C to 1420 °C and lower basicity range of 1.26 to 2.20.

Figure 9 shows the effect of dephosphorization slag basicity on the mass action concentration of calcium silicates. With increasing dephosphorization slag basicity, N_{CS} decreases exponentially, N_{C2S} increases first and then decreases, N_{C3S} increases exponentially and N_{C3S2} shows a decreasing trend as a whole. The variation trend of N_{CS}, N_{C2S} and N_{C3S} is consistent with the results obtained by Jingyan Li *et al.*[28] At the conditions of CaO-15 pct SiO_2-FeO-Fe_2O_3-5 pct P_2O_5 slag, 1450 °C to 1600 °C, basicity of 1.8 to 3.7. The increase of dephosphorization slag basicity can reduce N_{C3S2}, and there is no obvious mathematical relationship between them.

Figure 9 shows that N_{CS} and N_{C2S} are one order of magnitude higher than N_{C3S} and N_{C3S2}, indicating that the former two have strong reaction ability in the dephosphorization slag, being the main components in the dephosphorization slag. Between N_{CS} and N_{C2S}, the value of N_{C2S} is always higher than that of N_{CS}, which indicates that C_2S has the strongest reaction ability in the dephosphorization slag, and the phosphorus in hot metal is easier to combine with C_2S to form phosphorus containing solid solution.

With increasing dephosphorization slag basicity from 1.26 to 2.20, it is calculated that N_{C2P} varies from 7.52×10^{-7} to 2.88×10^{-6}, N_{C3P} varies from 0.012 to 0.026, and N_{C4P} varies from 2.14×10^{-5} to 2.20×10^{-4}. In addition, the variation range of N_{F3P} is 2.57×10^{-14} to 3.29×10^{-12}, the variation range of N_{F4P} is 4.32×10^{-14} to 6.90×10^{-12}, the variation range of N_{M2P} ranging from 3.13×10^{-10} to 8.43×10^{-9} and that of N_{M3P} from 3.58×10^{-9} to 5.82×10^{-8}. Considering the above range value, the variation range of N_{C2P}, N_{C4P}, N_{F3P}, N_{F4P}, N_{M2P} and N_{M3P} is less than 10^{-4} in the dephosphorization slag with the basicity from 1.26 to 2.20, so it is reasonable to ignore the effect of the above components on the phosphorus-enrichment effect. According to the above description, in the low temperature range of 1370 °C to 1420 °C and the low basicity range of 1.26 to 2.20, the P_2O_5 containing components in the dephosphorization slag mainly combined with calcium silicate are C_3P.

B. *Effect of Dephosphorization Slag Basicity on Phosphorus-Enrichment Contribution Ratio R_{Ci} of Calcium Silicate*

The phosphorus-enrichment contribution ratio R_{Ci} can well indicate the enrichment degree of P_2O_5 containing solid solution by different calcium silicate in slag.[27] According to Eq. [16], the phosphorus-enrichment contribution ratios of four kinds of calcium silicate of R_{CS}, R_{C2S}, R_{C3S} and R_{C3S2} are calculated. The effect of dephosphorization slag basicity on phosphorus-enrichment capacity of different calcium silicate in dephosphorization slag is further studied under the conditions of low temperature range of 1370 to 1420 °C and low basicity range of 1.26 to 2.20.

Figure 10 shows the changes in the phosphorus-enrichment contribution ratio R_{Ci} under different basicities of dephosphorization slags. From the proportion of different strip areas in Figure 10(a), it can be seen that

Table VII. Average Mass Fractions of Different Compositions in P-Rich Phase of Dephosphorization Slag and the Average Mass Fractions of C_iS and C_3P at Different Basicities/(Pct)

B	SiO_2	P_2O_5	CaO	FeO	MnO	MgO	Al_2O_3	C_3P	C_iS ($1<i<2$)
1.26	33.71	3.63	40.76	6.78	5.46	6.37	3.29	7.92	70.18
1.37	31.97	7.61	45.31	2.79	2.67	7.64	2.01	16.62	68.28
1.50	27.38	12.86	47.83	4.82	4.56	1.04	1.51	28.07	59.99
1.71	28.75	14.83	51.54	1.03	2.21	0.64	1.00	32.38	62.74
1.90	24.81	17.56	48.77	2.78	2.44	2.33	1.31	38.32	52.8
2.20	24.66	20.56	48.59	0.37	2.98	2.47	0.37	44.89	48.93

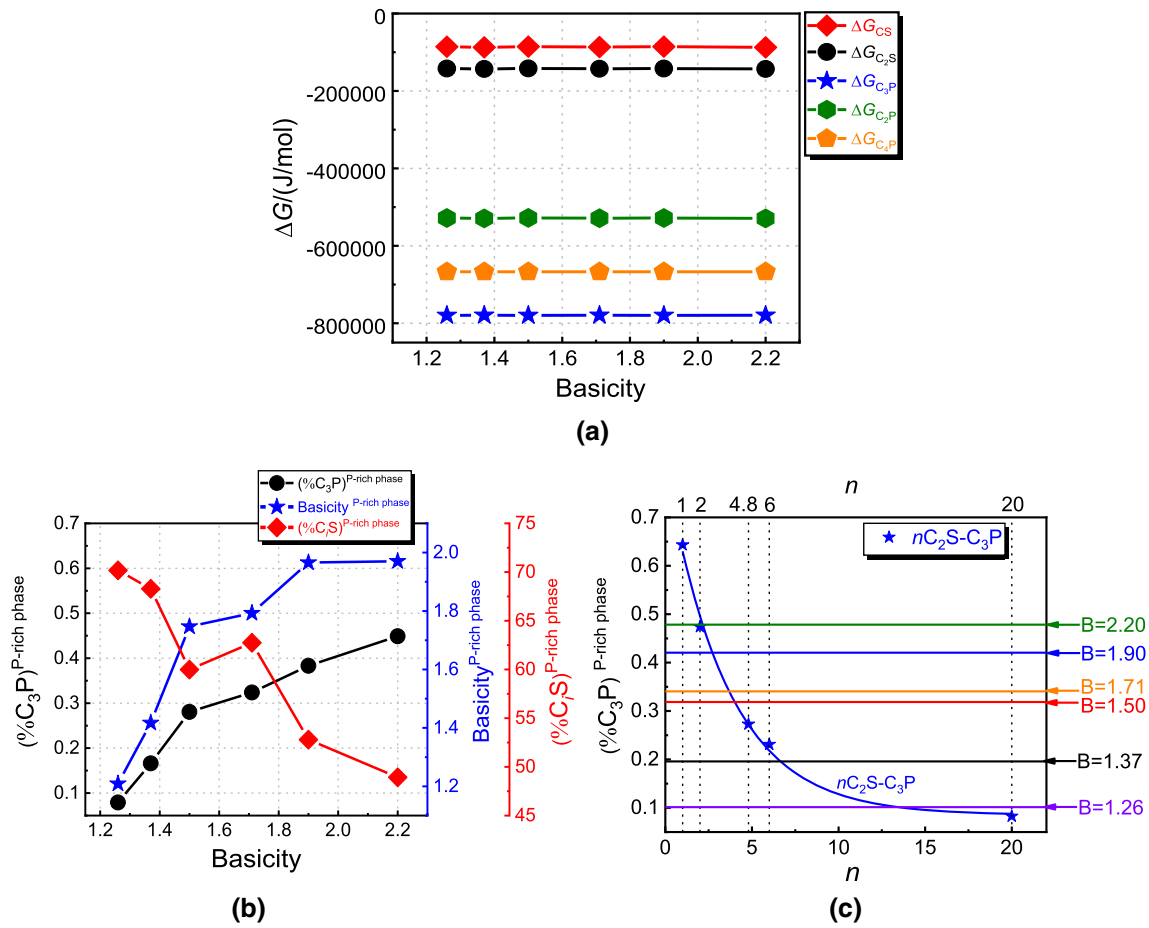

Fig. 7—(*a*) Gibbs free energy changes of C_iS ($i=1,2$) and C_jP ($j=1,2,3$) under different basicities of dephosphorization slag; (*b*) Effect of dephosphorization slag basicity on C_3P content, basicity, C_iS content in P-rich phase of dephosphorization slag; (*c*) Determination of coefficient n in nC_2S-C_3P of the P-rich phase at different basicities.

the phosphorus-enrichment contribution ratio of R_{C2S} is the largest. With increasing dephosphorization slag basicity from 1.26 to 2.20, the R_{C2S} increases from 0.56 to 0.84, the R_{CS} significantly reduces, and the value of R_{CS} decreases from 0.41 to 0.11, while the proportions of R_{C3S} and R_{C3S2} have very small values. This indicates that with increasing dephosphorization slag basicity, phosphorus tends to combine with C_2S to be enriched. It can be seen from Figure 10(b) and (c) that the change trend of R_{C2S} is the same as dephosphorization ratio, but the change trend of R_{CS} is opposite to dephosphorization ratio. Therefore, the increase of dephosphorization slag basicity mainly will increase the phosphorus-enrichment capacity of C_2S and decrease the phosphorus-enrichment capacity of CS.

The mathematical relationship between dephosphorization slag basicity and phosphorus-enrichment contribution ratio of calcium silicate are further studied. Figure 10(b-e) shows that with increasing dephosphorization slag basicity, R_{CS} and R_{C3S2} decrease exponentially, R_{C2S} and R_{C3S} increase exponentially. The regression coefficients, r^2, of R_{CS}, R_{C2S} and R_{C3S} against

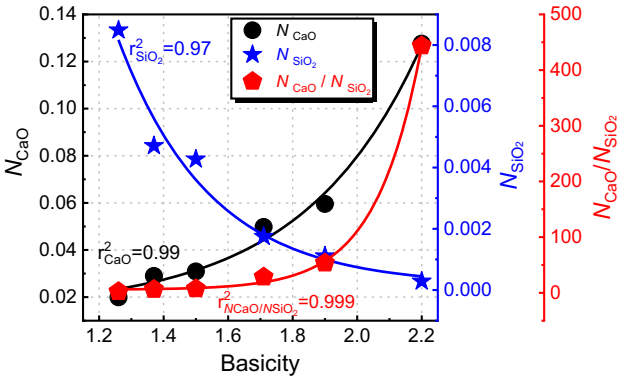

Fig. 8—Effect of dephosphorization slag basicity on N_{CaO}, N_{SiO_2} and N_{CaO}/N_{SiO_2}.

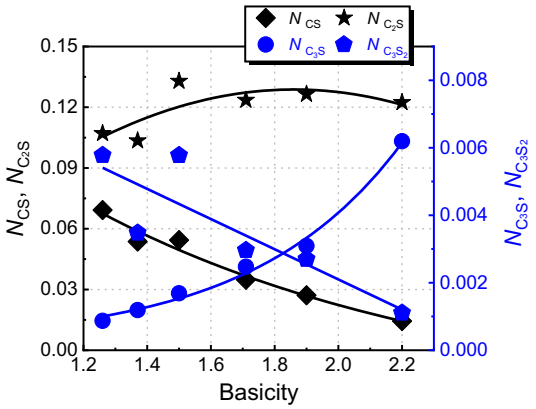

Fig. 9—Effect of dephosphorization slag basicity on the mass action concentration of calcium silicate of N_{CS}, N_{C2S}, N_{C3S} and N_{C3S2}.

dephosphorization slag basicity are greater than 0.99. There is an obvious exponential relationship between dephosphorization slag basicity and R_{CS}, R_{C2S} and R_{C3S}, which can be expressed by Eqs. [24] through [26]:

$$R_{CS} = 1.598 \times \exp(\frac{-B}{1.121}) - 0.11 \quad [24]$$

$$R_{C2S} = -1.835 \times \exp(\frac{-B}{0.854}) + 0.982 \quad [25]$$

$$R_{C3S} = 1.123 \times 10^{-4} \times \exp(\frac{B}{0.381}) + 0.0018 \quad [26]$$

C. *Effect of Dephosphorization Slag Basicity on Phosphorus-Enrichment Behavior*

It has been shown that C_2S is the main phosphorus-enrichment component in the dephosphorization slag. Therefore, the phosphorus-enrichment behavior of C_2S in the dephosphorization slag can represent the phosphorus-enrichment behavior in the dephosphorization slag. Based on the enrichment degree R_{Ci-Pj} of P_2O_5 containing solid solution, the effect of the dephosphorization slag basicity on the phosphorus-enrichment behavior of C_2S in dephosphorization slag was analyzed under the conditions of low temperature range of 1370 °C to 1420 °C and low basicity range of 1.26 to 2.20.

In the dephosphorization reaction of slag, CaO reacts with SiO_2 to generate C_2S. FeO and CaO react with P_2O_5 to form F_3P and C_3P, respectively, which initially fixes phosphorus in dephosphorization slag.[41] Further, P_2O_5 in F_3P is easy to react with CaO to form more stable C_3P,[27] the chemical reaction is expressed as Eq. [27]. According to the standard Gibbs free energy of the above reactions summarized in Table VI, the actual Gibbs free energy of F_3P reacting with CaO to produce C_3P is derived, which is expressed as Eq. [28]. The substituted FeO diffuses into CaO solid through the reaction interface and forms CaO-FeO layer.

$$3(CaO) + (3FeO \cdot P_2O_5) = 3(FeO) + (3CaO \cdot P_2O_5) \quad [27]$$

$$\Delta G_{F3P-C3P} = -279486 - 86.558T + RT\ln\left(\frac{(N\text{FeO})^3 \times (N_{3CaO\cdot P_2O_5})}{(N\text{CaO})^3 \times (N_{3FeO\cdot P_2O_5})}\right) \quad [28]$$

Under the conditions of lower temperature and lower basicity in the dephosphorization stage of the NDSP, the existence state of C_2S is α'_H-C_2S state,[42] and α'_H-C_2S mainly exists in the form of $2Ca^{2+}$ and $[SiO_4]^{4-}$. C_3P mainly exists in the form of $3Ca^{2+}$ and $2[PO_4]^{3-}$. The radii of $[SiO_4]^{4-}$ and $[PO_4]^{3-}$ are 2.79 Å and 2.76 Å, respectively, and their crystal structures are tetrahedral.[43] This shows that the structure and size of $[SiO_4]^{4-}$ and $[PO_4]^{3-}$ are very similar and can replace each. In the range of 1370 °C to 1420 °C, the Gibbs free energy of the reaction of CaO with P_2O_5 to produce C_3P is much smaller than that of the reaction of CaO with SiO_2 to produce C_2S. The affinity of CaO with P_2O_5 is much stronger than that with SiO_2. P can replace part of Si in the tetrahedral structure, resulting in the change of its coordination structure, which shows that $[PO_4]^{3-}$ replaces $[SiO_4]^{4-}$ in the solvent C_2S lattice.

Furthermore, $\Delta G_{F3P-C3P}$ is always less than 0 in the NDSP. C_2S-F_3P can not exist stably, and F_3P will spontaneously transform into C_3P. Therefore, it can be considered that the formation of C_2S-C_3P solid solution is through the replacement of $[SiO_4]^{4-}$ in C_2S phase by $[PO_4]^{3-}$ in slag, or transformation of the unstable C_2S-F_3P phase into the stable C_2S-C_3P.

Figure 11 shows the effect of dephosphorization slag basicity on $R_{C2S-C3P}$, $R_{C2S-C4P}$ and $R_{C2S-F3P}$. With increasing dephosphorization slag basicity, $R_{C2S-C3P}$, $R_{C2S-C4P}$ both increase exponentially, while $R_{C2S-F3P}$ decreases exponentially. This is because the increase of basicity will promote the formation of C_2S-C_3P solid solution in slag, and the coefficient n of nC_2S-C_3P solid solution will decrease with increasing basicity, thus improving the enrichment degree of phosphorus in C_2S-C_3P solid solution in dephosphorization slag. In

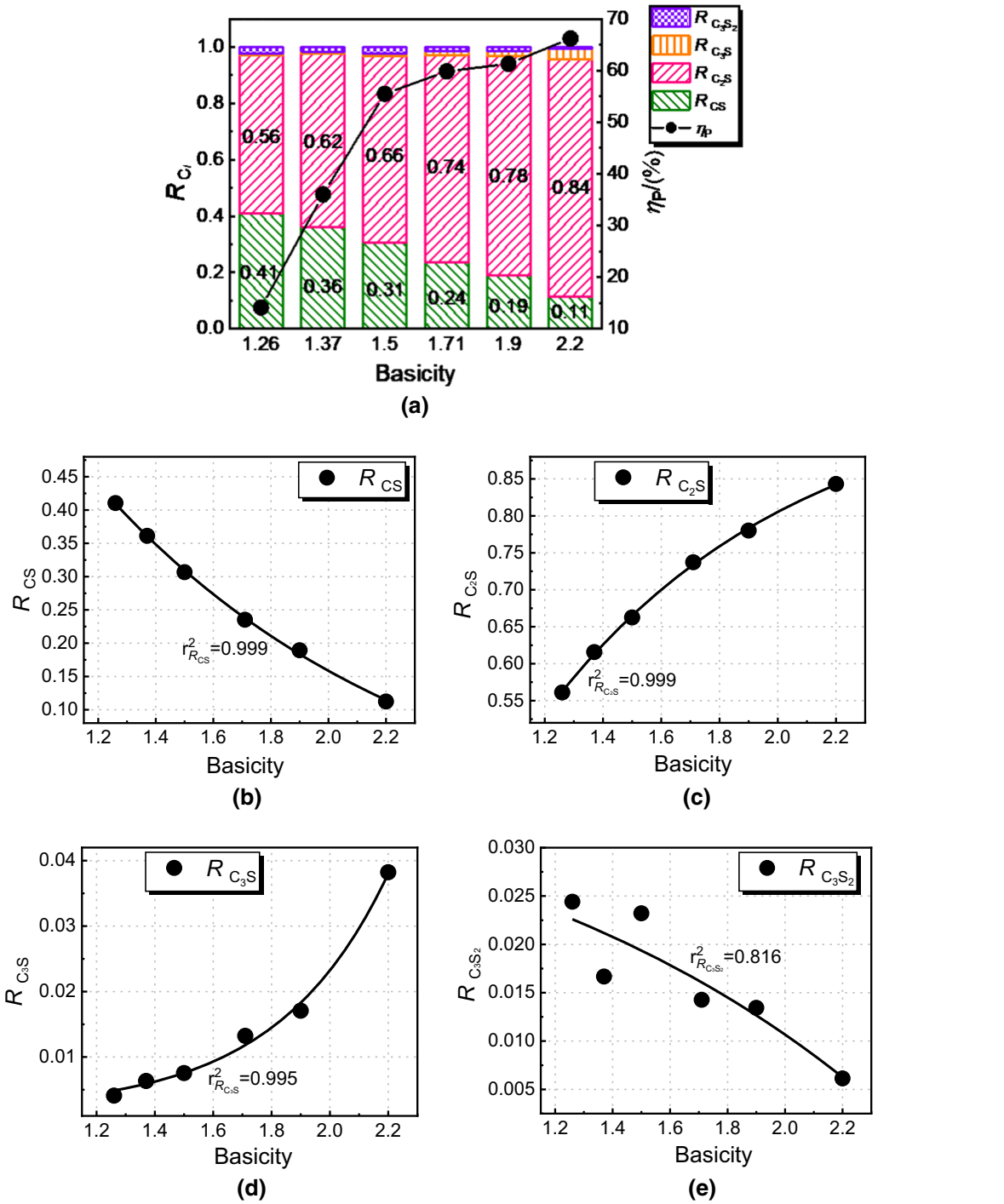

Fig. 10—Changes in the phosphorus-enrichment contribution ratio R_{Ci} under different basicities of dephosphorization slags. (*a*) Effect of dephosphorization slag basicity to the phosphorus-enrichment contribution ratio R_{Ci}; Effect of dephosphorization slag basicity on (*b*) R_{CS}, (*c*) R_{C2S}, (*d*) R_{C3S}, (*e*) R_{C3S2}.

addition, under the conditions of lower temperature and lower basicity in the dephosphorization stage of the NDSP, F_3P spontaneously transforms to C_3P, and with increasing dephosphorization slag basicity, this change trend will become more obvious. Therefore, it can be concluded that increasing dephosphorization slag basicity is beneficial to the enhancement of phosphorus-enrichment degree in dephosphorization slag, and the phosphorus-enrichment ability of C_2S-C_3P and C_2S-C_4P will be significantly improved.

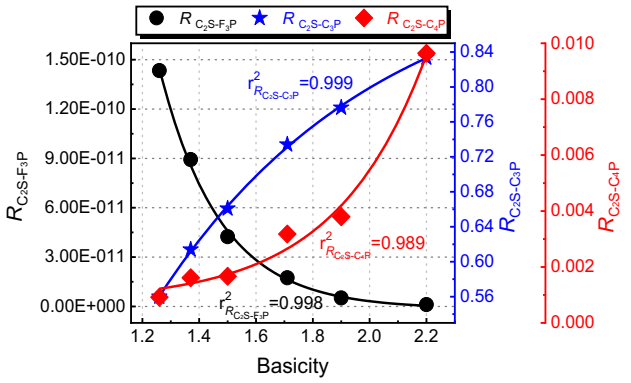

Fig. 11—Effect of dephosphorization slag basicity on $R_{C2S-C3P}$, $R_{C2S-C4P}$ and $R_{C2S-F3P}$.

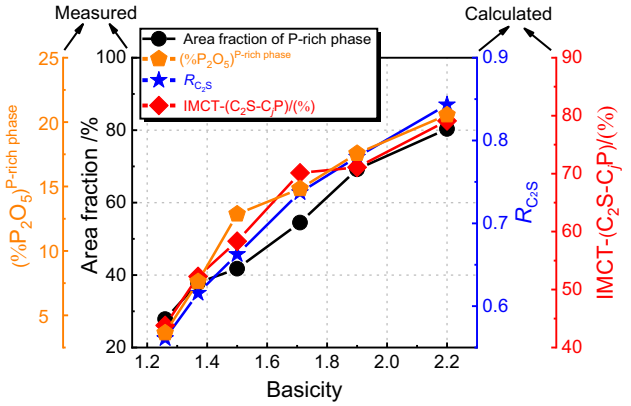

Fig. 12—Comparison between the calculated results of IMCT-(pct C_2S-C_jP) and R_{C2S}, and the measurement results of $A^{P\text{-rich phase}}$, and $(\text{pct } P_2O_5)^{P\text{-rich phase}}$ of industrial experiment.

D. *Comparison Between the Measurement Results of Industrial Experiment and the Calculated Results of IMCT*

In Section IV–C, the mass fraction of CaO, SiO_2 and P_2O_5 in the P-rich phase is analyzed by SEM-EDS. The sum of the mass fraction of CaO, SiO_2 and P_2O_5 represents the mass fraction of phosphorus containing solid solution in the P-rich phase, expressed as (pct C_iS-C_jP). According to the conclusion in Section V–C, C_2S is the main component of phosphorus enrichment in the dephosphorization slag. Therefore, the product of the mass fraction of phosphorus containing solid solutions (pct C_iS-C_jP) and the phosphorus-enrichment contribution ratio R_{C2S} of C_2S is regarded as the mass fraction of C_2S-C_jP solid solution in P-rich phase(IMCT-(pct C_2S-C_jP)), which is calculated by Eq. [29]. The areas of P-rich phase in dephosphorization slag with different basicities can be calculated using Image Pro Plus software under three viewing fields of SEM at the magnification of 1500 times, and Eq. [30] is used to calculate the average area fraction of P-rich phase($A^{P\text{-rich phase}}$). The calculated results of IMCT-(pct C_2S-C_jP) and R_{C2S} can illustrate the phosphorus-enrichment degree. Both the calculation results are compared with the measurement results of $A^{P\text{-rich phase}}$, and $(\text{pct } P_2O_5)^{P\text{-rich phase}}$ to verify the rationality of the IMCT calculation results.

$$\text{IMCT} - (\%C_2S - C_jP) = (\%C_iS - C_jP)^{P\text{-rich phase}} \times R_{C_2S} \quad [29]$$

$$A^{P\text{-rich phase}} = \frac{\text{Area}^{P\text{-rich phase}}}{\text{Area}^{\text{Total field of view}}} \quad [30]$$

Figure 12 shows the comparison between the calculated results of IMCT-(pct C_2S-C_jP) and R_{C_2S}, and the measurement results of $A^{P\text{-rich phase}}$, and $(\text{pct } P_2O_5)^{P\text{-rich phase}}$ of industrial experiment. With increasing dephosphorization slag basicity, IMCT calculated results and experimental results are all increased. The trends of the enrichment degree of phosphorus in dephosphorization slag are well consistent among the results characterized by different ways. Therefore, the IMCT calculated results can correctly express the phosphorus-enrichment degree of dephosphorization slag, and further reveal the phosphorus-enrichment degree of the different calcium silicates in dephosphorization slag.

VI. CONCLUSIONS

In the percent work, the dephosphorization experiments using new double slag converter steelmaking process(NDSP) has been carried out in a 180 ton top-bottom combined blowing converter under the low temperature range of 1370 °C to 1420 °C and low basicity of 1.26 to 2.20. Based on the ion-molecule coexistence theory (IMCT) and phase analysis of dephosphorization slag, the effect of dephosphorization slag basicity on the hot metal dephosphorization and the phosphorus-enrichment behavior in slag is studied, and the following conclusions are obtained:

1. With increasing basicity, the phosphorus distribution ratio L_P between hot metal and slag increases. The dephosphorization ratio and the decarbonization ratio both increase, while the demanganization ratio decreases. The desiliconization ratio has no obvious change and remains at a high level. When the basicity is 2.20, the phosphorus content in hot metal decreases from 0.142 to 0.048 pct, the dephosphorization ratio increases to 66.2 pct and the phosphorus distribution ratio increases to 81.33.
2. With increasing basicity from 1.26 to 2.20, the morphologies of P-rich phase change from long strip shape (B = 1.26 to 1.37) to dendritic shape (B = 1.50) and to massive shape(B = 1.71 to 2.20). The area of P-rich phase increases from about 4 μm^2 to about 8000 μm^2. The content of P_2O_5 in the P-rich phase increases and the value of the coefficient n in nC_2S-C_3P of P-rich phase decreases from 6-20 to 1-2.
3. With increasing basicity, N_{CaO} and N_{SiO_2} increases and decreases exponentially, respectively, and

N_{CaO}/N_{SiO_2} also increases exponentially. The phosphorus-enrichment contribution ratio of calcium silicate is in the order of $R_{C2S}>R_{CS}>R_{C3S}>R_{C3S2}$. C_2S is the main phosphorus-enrichment calcium silicate in dephosphorization slag, and R_{C2S} has the value of 0.56 to 0.84. The phosphorus-enrichment degree in dephosphorization slag is enhanced mainly by C_2S-C_3P.

4. In the dephosphorization stage of the NDSP, C_2S is in the existence state of α'H-C_2S state. The formation of C_2S-C_3P solid solution is through the replacement of $[SiO_4]^{4-}$ in C_2S phase by $[PO_4]^{3-}$ in slag, or transformation of the unstable C_2S-F_3P phase into the stable C_2S-C_3P.
5. With increasing basicity, the calculated results of IMCT-(pct C_2S-C_jP) and R_{C2S} are well consistent with the measurement results of $A^{\text{P-rich phase}}$ and (pct P_2O_5)$^{\text{P-rich phase}}$ of industrial experiment, indicating that the IMCT calculated results can correctly express the phosphorus-enrichment degree of dephosphorization slag. It is possible to use the enrichment contribution ratio R_{Ci} to qualitatively predict the phosphorus-enrichment degree of calcium silicate in dephosphorization slag.
6. From the present results, it is reasonable to deduce that the method combining laboratory phase analysis and IMCT thermodynamic calculation can facilitate optimizing the dephosphorization process parameters of NDSP under low temperature and low basicity, which has a guiding significance for industrial production.

ACKNOWLEDGMENTS

The work was financially supported by the National Natural Science Foundation of China (U1960202).

CONFLICT OF INTEREST

On behalf of all authors, the corresponding author states that there is no conflict of interest.

ABBREVIATIONS

a_i, b_i	Initial mole numbers of component i in 100 g dephosphorization slag, (mol)
$\sum n_i$	Total equilibrium moles of all structural units in 100 g dephosphorization slag based on IMCT, (mol)
N_i	Mass action concentration of structural unit i or ion couple i in dephosphorization slag based on IMCT, (−)
$\Delta_r G^{\Theta}_{m,ci}$	Change of standard molar Gibbs free energy of reaction for structural unit i or component i, (J/mol)
K^{Θ}_{ci}	Standard equilibrium constants of chemical reactions for forming component i or structural unit i, (−)
M_i	Relative atomic mass of element i or the relative molecular mass of component i, (−)
N_{Ci-Pj}	Defined-enrichment possibility of containing P_2O_5 solid solution based on the calculated mass action concentration N_i of complex molecule C_i and P_j, (−)
R_{Ci-Pj}	Enrichment degree of solid solution containing P_2O_5 based on IMCT, (−)
R_{Ci}	Phosphorus-enrichment contribution ratio of calcium silicate based on IMCT, (−)
η_i	Removal ratio of elements in hot metal, (pct)
T	Temperature, (°C)
B	Binary basicity, (−)
r^2	Fitting regression coefficient, (−)
$n(i)^{\text{P-richphase}}$	Mole number of i in P-rich phase, (mol)
ΔG_{A-B}	Actual Gibbs free energy of A to B reaction, (J)
IMCT-(pct C_2S-C_jP)	Mass fraction of C_2S-C_iP solid solution in P-rich phase by IMCT, (pct)
$A^{\text{P-rich phase}}$	Average area fraction of P-rich phase at 1500 times under 3 fields of view, (pct)

REFERENCES

1. Y Ogawa, M Yano, SY Kitamura, and H Hirata: *Tetsu-to-Hagané*, 2001, vol. 87 (1), pp. 21–28.
2. Y Ogawa, M Yano, SY Kitamura, and H Hirata: *Steel Res. Int.*, 2003, vol. 74 (2), pp. 70–76.
3. N Sasaki, Y Ogawa, S Mukawa, and KI Miyamoto: *Nippon Steel Tech. Rep.*, 2012, vol. 394, pp. 26–32.
4. Y Wang, SF Yang, JS Li, J Feng, and F Wang: *High Temp. Mater. Proc.*, 2018, vol. 37 (7), pp. 625–33.
5. WK Yang, J Yang, YQ Shi, ZJ Yang, FB Gao, RH Zhang, and GF Ye: *Ironmak. Steelmak.*, 2020, https://doi.org/10.1080/03019233.2020.1731256.
6. YR Fang, BC Huang, ZY Lai, BY Chen, and XF Zeng: *Steelmaking*, 2014, vol. 30 (3), pp. 1–4.
7. FY Liu, GC Wang, Y Zhao, JW Tan, CM Zhao, and Q Wang: *Ironmak. Steelmak.*, 2019, vol. 46 (4), pp. 392–403.
8. ML Wang and WY Yang: *Ironmak. Steelmak.*, 2019, https://doi.org/10.1080/03019233.2019.1673546.
9. G. F. Ye, J. Yang, R, H, Zhang, W. K. Yang and H. Sun: *Int. J. Miner. Metall. Mater.*, 2021, vol. 28(1), pp. 66-75.
10. SL Xie and WL Wang: *Steel Res. Int.*, 2016, vol. 87 (3), pp. 376–85.

11. SL Xie, WL Wang, ZC Luo, and DY Huang: *Metall. Mater. Trans. B.*, 2016, vol. 47B, pp. 1583–93.
12. S Kakimoto, A Kiyose, and R Murao: *ISIJ Int.*, 2017, vol. 57 (10), pp. 1710–17.
13. CM Du, NN Lv, C Su, WM Liu, JX Yang, and HC Wang: *J. Iron Steel Res. Int.*, 2019, vol. 26, pp. 1162–70.
14. PK Son and Y Kashiwaya: *ISIJ Int.*, 2008, vol. 48 (9), pp. 1165–74.
15. S Fukagai, T Hamano, and F Tsukihashi: *ISIJ Int.*, 2010, vol. 47 (1), pp. 187–89.
16. R Inoue and H Suito: *ISIJ Int.*, 2006, vol. 46 (2), pp. 174–79.
17. R Inoue and H Suito: *ISIJ Int.*, 2006, vol. 46 (2), pp. 180–87.
18. XC Ma, GG Cheng, and J Zhang: *J. Univ. Sci. Technol. Beijing.*, 2011, vol. 33 (11), pp. 1337–40.
19. GG Cheng and J Zhang: *Iron Steel Vanadium Titanium*, 1994, vol. 15 (3), pp. 1–2.
20. GG Cheng and J Zhang: *Iron Steel Vanadium Titanium*, 1994, vol. 15 (2), pp. 1–4.
21. GG Cheng and P Zhao: *J. Univ. Sci. Technol. Beijing.*, 1995, vol. 17, pp. 52–56.
22. XM Yang, JP Duan, CB Shi, M Zhang, YL Zhang, and JC Wang: *Metall. Mater. Trans. B.*, 2011, vol. 42B, pp. 738–70.
23. XM Yang, CB Shi, M Zhang, JP Duan, and J Zhang: *Metall. Mater. Trans. B.*, 2011, vol. 42B, pp. 951–76.
24. NM Chuiko: *Ferrous Met.*, 1959, vol. 5, pp. 3–10.
25. J Zhang: *Computational Thermodynamics of Metallurgical Melt and Solutions*, Metallurgical Industry Press, Beijing, 2007.
26. PC Li, XM Yang, and J Zhang: *J. Univ. Sci. Technol. Beijing.*, 2014, vol. 36 (12), pp. 1608–14.
27. SL Xie, WL Wang, DY Huang, HC Li, and Y Du: *Steel Res. Int.*, 2018, vol. 89, p. 1700317.
28. JY Li, M Zhang, M Guo, and XM Yang: *Metall. Mater. Trans. B.*, 2014, vol. 45B, pp. 1666–82.
29. JY Li, M Zhang, M Guo, and XM Yang: *Int. J. Miner. Metall. Mater.*, 2016, vol. 23 (5), pp. 520–33.
30. W. K. Yang, J. Yang, Y. Q. Shi, Z. J. Yang, F. B. Gao, R. H. Zhang and G. F. Ye: *Steel Res. Int.*, 2021, vol. 92. https://doi.org/10.1002/srin.202000438.
31. W.K. Yang, J. Yang, Y.Q. Shi, Z.J. Yang, F.B. Gao, R.H. Zhang and H. Sun: *Metals*, 2021, vol. 11. https://doi.org/10.3390/met11030417.
32. X. Han, C.G. Zhou, J. Li, C.B. Shi, J.P. Ge and K.S. Cai: *J. Iron Steel Res.,* 2016, vol. 28(9), pp. 40-49.
33. W.L. Dong, H.W. Pan, L. Luo, C.X. Ji, H.B. Li and Z.H. Tian: *Iron and Steel*, 2020, vol. 55(2), pp. 75-81, 94.
34. XH Huang: *Principles of Iron and Steel Metallurgy*, Metallurgical Industry Press, Beijing, 2002.
35. W Xiong, J Wang, and F Yang: *Mining Metallurgy*, 2013, vol. 22 (4), pp. 47–50.
36. C Li, HJ Guo, and GG Cheng: *Special Steel*, 2009, vol. 30 (5), pp. 4–6.
37. Y Liu, SH Peng, YJ Xia, and XB Zhou: *J. Univ. Sci. Technol. Anhui.*, 2019, vol. 36 (1), pp. 7–12.
38. DZ Wang, YP Bao, and M Wang: *Chin. J. Eng.*, 2018, vol. 40 (1), pp. 65–72.
39. M Timucin and A Muan: *J. Am. Cream. Soc.*, 1922, vol. 75, pp. 1399–1406.
40. I Barin, O Knacke, and O Kubaschewski: *Thermochemical Properties of Inorganic Substances*, Springer, Berlin, 1977.
41. SY Kitamura, S Saito, K Utagawa, H Shibata, and DGC Robertson: *ISIJ Int.*, 2009, vol. 49 (12), pp. 1838–44.
42. WS Zhang, JT Zhang, JY Ye, JS Qian, WG Shen, and ZY Wang: *J. Chin. Ceram. Soc.*, 2019, vol. 47 (11), pp. 1664–69.
43. B Dikens and WE Brown: *Tsehermaks Min. Petr. Mitt.*, 1971, vol. 16, pp. 1–27.